Linear stability of natural convection in a differentially heated shallow cavity submitted to high-frequency horizontal vibrations

Abdessamed Medelfef, Daniel Henry, Slim Kaddeche, Faiza Mokhtari, Samia Bouarab, Valéry Botton, Ahcene Bouabdallah

Linear stability of natural convection in a differentially heated shallow cavity submitted to high-frequency horizontal vibrations

Abdessamed Medelfef*[1], Daniel Henry[2], Slim Kaddeche[3], Faiza Mokhtari[1], Samia Bouarab[4], Valéry Botton[2] and Ahcene Bouabdallah[1]

[1] *Laboratoire de Thermodynamique et Systèmes Energétiques, Faculté de Physique, Université des Sciences et de la Technologie Houari Boumediène, BP 32, 16111 Bab Ezzouar, Alger, Algérie*
[2] *Laboratoire de Mécanique des Fluides et d'Acoustique, CNRS, Université de Lyon, Ecole Centrale de Lyon/ Université Lyon 1/INSA Lyon, ECL, 36 Avenue Guy de Collongue, 69134 Ecully Cedex, France*
[3] *Laboratoire de Recherche Matériaux, Mesures et Applications LR-11-ES-25, Institut National des Sciences Appliquées et de Technologie, BP 676, 1080 Tunis Cedex, Tunisie*
[4] *Université M'hamed Bougara, Avenue de l'indépendance, 35000, Boumerdès, Algérie*

July 14, 2023

Abstract

This study concerns the linear stability of buoyant convection induced by lateral heating inside a shallow cavity. It highlights the effects caused by submitting the flow to horizontal high-frequency vibrations. The steady-state profiles are first derived using a parallel flow approximation and studied for two types of boundaries, either thermally insulating or thermally conducting. The basic flow is found to be attenuated when subjected to horizontal high-frequency vibrations, with a faster decay in the case of thermally insulating walls than in the case of thermally conducting walls. The effects of vibrations and thermal boundary conditions are then investigated for various types of instability that may arise in such a situation, depending on the Prandtl number, such as shear, oscillatory, and thermal instabilities. It is observed that horizontal high-frequency vibrations have a stabilizing effect on all instabilities developing in such a situation and that this stabilization is generally more efficient in the case of insulating walls, for which the basic flow is attenuated more rapidly. We finally analyze the physical mechanisms that trigger these instabilities through fluctuating energy budgets at the critical thresholds.

*Corresponding author: abs.medelfef@gmail.com

1 Introduction

Buoyant convection induced by a horizontal gradient of temperature is a canonical problem of fluid mechanics because of its presence in various natural and practical situations. Among these situations is the horizontal Bridgman crystal growth process, where a low Prandtl number fluid inside a crucible is pulled in a furnace with a horizontal temperature gradient. The melt is the seat of a buoyancy-driven flow, which may undergo instabilities that will be captured in the solid phase structure as the solidification front advances, inducing thus a degradation of the crystal quality (Dhanaraj et al., 2010; Kaddeche et al., 2015).

In the case of extended cavities, this buoyant flow consists of a long single cell, called Hadley circulation (Hadley, 1735), which can be well approximated by a simple steady parallel flow model. One of the first stability studies conducted on the cubic velocity profile, along the vertical direction, obtained with this model was carried out by Hart (1972). His work was further deepened by Laure (1987) and Laure and Roux (1989). In these studies (Hart, 1972; Laure, 1987; Laure and Roux, 1989), two types of instabilities were studied: a shear instability developing at very low Prandtl numbers, which consists of a two-dimensional transverse stationary mode, and an oscillatory instability at moderate Prandtl numbers developing as a three-dimensional longitudinal mode. For larger Prandtl numbers, in the case of thermally conducting boundaries, Gershuni et al. (1992) found a third instability type, which consists of Rayleigh-Bénard three-dimensional longitudinal stationary rolls developing near the horizontal walls where the temperature profile produces a region of unstable stratification. In contrast, for thermally insulating walls, Kuo and Korpela (1988) found that the instability sets in as three-dimensional stationary longitudinal rolls of shear origin. Delgado-Buscalioni and Crespo del Arco (1999) analyzed the linear and non-linear stability of the buoyancy-driven flow in an inclined cavity for different tilt angles and a wide range of Prandtl numbers. Their study shows that, depending on the value of the Prandtl number, the basic steady flow may break down due to shear rolls or long-wave oscillatory instabilities. In addition to these studies, Pimputkar and Ostrach (1981), and more recently Lappa (2007), presented extensive reviews concerning the stability of buoyant convection driven by a horizontal temperature gradient in shallow horizontal cavities, where different effects, such as thermal or dynamical boundary conditions, capillary forces, and the ability of the fluid to diffuse heat (Prandtl number), have been considered.

These previous studies have shown the existence of different instability modes, which arise from diverse physical mechanisms, such as shear or buoyancy. Consequently, this makes the Hadley flow a canonical model to investigate the control of natural convection flow using various techniques such as magnetic field, acoustic streaming, rotation, or even vibrations. The effect of the magnetic field on the buoyancy-driven flow and its stability has been first studied by Kaddeche et al. (2003) and Henry et al. (2005) for different orientations of the field, with low to moderate intensities. More recently, the effect of strong magnetic fields has been analyzed by Hudoba et al. (2016) and other instability modes related to Hartmann boundary layers are retrieved. Moreover, the effect of the Prandtl number on these instabilities has also been investigated by Hudoba and Molokov (2018).

Dridi et al. (2008, 2010) investigated the effect of ultrasonic waves producing an acoustic streaming flow on the stability of Hadley flow. The generation of an acoustic streaming flow modifies the structure of the basic flow, thus causing a drastic change in its stability, notably by the appearance of other instabilities connected to the acoustic streaming shear flow.

The effect of rotation around the vertical axis parallel to gravity has been studied by Shvarts (2005), Shvarts and Boudlal (2010), Chikulaev and Shvarts (2015), Medelfef et al. (2017), and Perez-Espejel and Avila (2019). These studies show that the intensity of the velocity profile decreases under rotation and that the parallel flow becomes composed of two horizontal components: a longitudinal component created by the longitudinal temperature gradient and a transverse component caused by the rotation. These changes lead to the development of oblique modes rather than longitudinal or transverse modes. All these instability modes, however, are stabilized by the action of the rotation and this stabilizing effect is even more pronounced, for each instability mode, when the Prandtl number increases.

The use of vibrations can also be interesting to control heated flows during solidification processes (Capper and Zharikov, 2015), conducted for example by the Czochralski or floating-zone methods (Lyubimov et al., 1997) or by the two horizontal and vertical Bridgman techniques (Lyubimova et al., 2014; Bouarab et al., 2020). Several studies have been conducted on such thermovibrational convection, both numerically and experimentally. When the heated system is submitted to high-frequency vibrations, the flow created by buoyancy may be subject to crucial modifications of its equilibrium properties. Changes can also occur when no gravity force exists, i.e., in weightlessness or microgravity conditions, with the creation of flows only due to vibrations. The reader can consult the reference textbook of Gershuni and Lyubimov (1998), Gershuni being one of the outstanding scientists who worked on the subject (Gershuni and Zhukhovitskii, 1963; Gershuni et al., 1970; Gershuni and Zhukhovitskii, 1981; Gershuni et al., 1982; Demin et al., 1996).

Following Gershuni's pioneering work on thermovibrations, the interactions between heated fluids and vibrations have been the subject of numerous research efforts in different situations to understand the mechanisms and the dynamics of the resulting flows. Some of these studies focused on the situation heated from below, i.e., the Rayleigh-Bénard configuration. For example, experimental investigations by Rogers et al. (2000), Zyuzgin et al. (2007), and Swaminathan et al. (2018) reported the effects of harmonic vibrations on the stability of a fluid layer heated from below, with a good agreement with the predictions of the linear stability theory. Gravity modulations have also been considered for fluid layers either heated from below (Gershuni and Zhukhovitskii, 1963; Gershuni et al., 1970) or heated from above or below (Gresho and Sani, 1970). Gresho and Sani (1970) showed that the stability limits could be strongly modified according to each situation. Further numerical studies on the effect of tilted high-frequency vibrations on the linear stability of such a situation were performed in the case of a porous cell (Bardan and Mojtabi, 2000), in an infinite fluid layer or a bounded rectangular enclosure (Cisse et al., 2004), and under a vertical magnetic field (Benzid et al., 2009).

The condition for the vibrations to be able to trigger convective flows even in reduced-gravity or weightlessness conditions is that the fluid is not uniformly heated. In such a situation, there is no exact equilibrium state with zero flow, but rather an averaged steady quasi-equilibrium state (Gershuni and Zhukhovitskii, 1981). Gershuni et al. (1982) were the first to study this flow in a rectangular cavity using numerical simulations. They obtained a variety of convection regimes when vertical high-frequency vibrations were applied. Experimental evidence has been reported for the first time by Mialdun et al. (2008) and Shevtsova et al. (2010) in a situation where a fluid cell, heated from above, is placed onboard the Airbus A300 Zero-G flight. Their results allowed to confirm the theoretical predictions reported in previous numerical studies. More recently, Perminov et al. (2022) studied thermovibrational convection under microgravity conditions in a laterally heated square cavity submitted to vertical high-frequency vibrations. According to the problem parameters, several convection modes have been observed, including a stationary structure with one to four rolls, and, eventually, an oscillatory convection is obtained for stronger heating conditions. Moreover, Crewdson and Lappa (2022) examined the effect of the thermal boundary conditions on thermovibrational convection in a cubic cavity under vertical high-frequency vibrations. A detailed characterization of the convective structures shows that the three-dimensional nature of the problem and its sensitivity to the thermal boundary conditions can remarkably influence the multiplicity of the emerging solutions and the temporal behavior of the system.

In the last few decades, particular attention has been brought to the influence of vibrations on natural convection due to lateral heating, because of the implication of these vibrations in different practical situations, such as the control of crystal growth processes (Bouarab et al., 2020). Indeed, the effect of vertical vibrations on transient convection in a square cavity is studied by Fu (1993), who shows that a steady quasi-equilibrium state is reached when high-frequency vibrations are introduced. Farooq and Homsy (1994) studied the flow in a laterally heated square cavity under a constant gravity field modulated by small harmonic oscillations. The same authors also studied the stability of the buoyancy-driven flow occurring in a laterally heated, vertically infinite fluid layer (Farooq and Homsy, 1996), and the effects of vibration were investigated using a Floquet approach. Furthermore, Demin et al. (1996) investigated the convection due to lateral heating in an infinite and inclined fluid layer, under high-frequency vibrations with arbitrary orientation. In the different configurations, depending on the tilt of the layer and the orientation of the vibrations, the conditions under which a mechanical quasi-equilibrium exists are specified and the linear stability boundaries and critical characteristics are then determined. Using direct numerical simulations, Lizée and Alexander (1997) studied the transition scenario of convection in a square cavity with differentially heated vertical walls under horizontal vibrations and showed that the transitions occur through a sequence of bifurcations following a Feigenbaum-type scenario. The particular case of an infinite fluid layer bounded by rigid and perfectly conducting walls and subjected to horizontal vibrations has been considered by Birikh and Katanova (1998). The different instability modes are found to be stabilized by the longitudinal vibrations, which act on the basic flow and on the disturbances. This stabilization, however, depends on the Prandtl number and on the instability mode, corresponding to plane or spiral perturbations, either stationary or oscillatory.

More recently, the influence of tilted high-frequency vibrations on the steady buoyant convection driven by lateral heating was studied by Bouarab et al. (2019) for an elongated rectangular cavity with an aspect ratio of 4 and by Mokhtari et al. (2020) for a cubic cavity. In these works, the stability of the flows was not considered, and performing such stability studies is one of the objectives in our team. To begin, the present study considers the stability of the parallel convective flow, driven by a horizontal temperature gradient in a laterally heated shallow cavity, and submitted to horizontal high-frequency vibrations, parallel to the temperature gradient. This is an extension of the work of Birikh and Katanova (1998) with the consideration of different thermal boundary conditions, the precise analysis of the influence of the vibrations and the Prandtl number on the different instabilities, the physical analysis of the instabilities through fluctuating energy budgets at threshold.

The paper is organized as follows. After the introduction, the second section is devoted to the mathematical model and the derivation and analysis of the basic steady-state flow solution. The linearized equations and the stability analysis techniques are then presented in the third section, before the derivation of the fluctuating energy budgets. Finally, the fifth section is devoted to the stability results, with a detailed analysis of the effects caused by the high-frequency vibrations on the different instabilities, depending on the thermal boundary conditions and the Prandtl number. Fluctuating energy budgets at threshold are also presented for each unstable mode in order to identify the physical mechanisms triggering the instabilities.

2 Governing equations and basic flow

We consider the buoyancy-driven flow of a Boussinesq Newtonian fluid enclosed between two infinite horizontal walls separated by a distance H. The kinematic viscosity ν and thermal diffusivity κ are supposed to be constants while the fluid density ρ varies linearly with temperature according to the Boussinesq approximation $\rho = \rho_0 \left[1 - \beta \left(\tilde{T} - \tilde{T}_0\right)\right]$, where β is the thermal expansion coefficient and $\left(\tilde{T}_0, \rho_0\right)$ are reference temperature and density, respectively. When the cavity is subjected to horizontal high-frequency harmonic vibrations along x, this induces a gravitational-like acceleration of the form $\vec{g} = \vec{g}_0 + b\,\Omega^2 \sin(\Omega t)\,\vec{e}_x$ where $\vec{g}_0$, $\vec{e}_x$, b and Ω stand for the static gravity acceleration, the unit vector indicating the vibrations direction, their amplitude, and finally their angular frequency, respectively, and t is the time. A sketch of the studied configuration and the system of coordinates is given in figure 1.

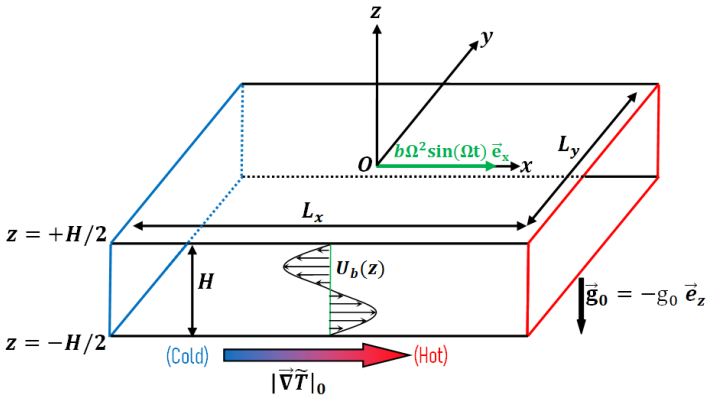

Figure 1: Sketch of the studied configuration and the system of coordinates.

2.1 Mathematical model

In the case of high-frequency vibrations, the mathematical model is given by the following set of equations (Gershuni and Lyubimov, 1998)

$$\frac{\partial \vec{U}}{\partial t} + (\vec{U}\cdot\vec{\nabla})\vec{U} = -\vec{\nabla}P + \Delta\vec{U} + Gr\,T\vec{e}_z + \frac{Gs}{Pr}\,(\vec{W}\cdot\vec{e}_x)\,\vec{\nabla}T, \tag{1a}$$

$$\frac{\partial T}{\partial t} + (\vec{U}\cdot\vec{\nabla})T = \frac{1}{Pr}\Delta T, \tag{1b}$$

$$\vec{\nabla}\times\vec{W} = \vec{\nabla}T\times\vec{e}_x, \tag{1c}$$

$$\vec{\nabla}\cdot\vec{U} = 0, \tag{1d}$$

$$\vec{\nabla}\cdot\vec{W} = 0. \tag{1e}$$

where H, H^2/ν, ν/H, $\rho_0\nu^2/H^2$, and $H|\vec{\nabla}\tilde{T}|_0$ have been used as scales for length, time, velocity, pressure, and temperature, respectively. $\vec{U}(U_x, U_y, U_z)$ is the velocity, T is the temperature, $\vec{W}(W_x, W_y, W_z)$ is the solenoidal part of $T\vec{e}_x$ (also known as the pulsation velocity), and P represents the pressure field.

Three dimensionless parameters characterize the studied problem: the Grashof number Gr, the Prandtl number Pr, and the Gershuni number Gs. They are given by the following expressions:

$$Gr = \frac{g_0\,\beta\,|\vec{\nabla}\tilde{T}|_0\,H^4}{\nu^2} \qquad Pr = \frac{\nu}{\kappa} \qquad Gs = \frac{\left(b\,\Omega\,\beta\,|\vec{\nabla}\tilde{T}|_0\,H^2\right)^2}{2\,\nu\,\kappa}.$$

Note that the Gs number is the analog of the vibrational Rayleigh number and has been noted in this way by several authors (Naumann et al., 2002; Shevtsova et al., 2010) to mark Gershuni's significant contribution to the study of flows under vibration.

2.2 Basic steady state profiles

In this section, we consider the basic steady state buoyancy-driven flow occurring in a cavity whose height H is small in comparison with the horizontal dimensions, i.e., $H \ll (L_x, L_y)$ (See Fig. 1). In this case, the flow induced by the horizontal temperature gradient along x between the two infinite horizontal walls is assumed to return at vertical boundaries located far from the center in the x and y directions and to be anti-symmetric with respect to the center located at $z = 0$. In such a situation, the mathematical model (Eqs (1a)-(1e)) admits a steady parallel flow solution which can be expressed as $\vec{U}_b = (U_b(z), 0, 0)$, $\vec{W}_b = (W_b(z), 0, 0)$, and $T_b = x + \Theta_b(z)$.

The pulsation velocity $\vec{W}_b$ is first obtained from Eq. (1c):

$$W_b(z) = \Theta_b(z). \tag{2}$$

The equation of motion (1a) then allows to derive the following system of equations:

$$\frac{d^2U_b(z)}{dz^2} + \frac{Gs}{Pr}\, W_b(z) = \frac{\partial P_b}{\partial x}, \tag{3a}$$

$$\frac{\partial P_b}{\partial y} = 0, \tag{3b}$$

$$Gr\ [x + \Theta_b(z)] + \frac{Gs}{Pr}\, W_b(z) \frac{d\Theta_b(z)}{dz} = \frac{\partial P_b}{\partial z}. \tag{3c}$$

The derivation of Eq. (3c) with respect to x, followed by integration along z, allows to get $dP_b/dx = Gr\, z$. Using Eq. (2), Eq. (3a) then gives a second-order differential equation for $U_b(z)$:

$$\frac{d^2U_b(z)}{dz^2} + \frac{Gs}{Pr}\, \Theta_b(z) = Gr\, z, \tag{4}$$

which is coupled with a second-order differential equation for $\Theta_b(z)$:

$$\frac{d^2\Theta_b(z)}{dz^2} = Pr\, U_b(z), \tag{5}$$

obtained from the energy equation (1b).

The set of coupled ODEs (4)-(5) is similar to that given by Gershuni and Lyubimov (1998) in the case of horizontal vibrations. The boundary conditions associated with these equations are $U_b(z = \pm 1/2) = 0$, ensuring the no-slip boundary condition, and either $\Theta_b(z = \pm 1/2) = 0$ for perfectly conducting walls (C-BC for conducting boundary conditions) or $(d\Theta_b/dz)_{(z=\pm 1/2)} = 0$ for perfectly insulating walls (I-BC for insulating boundary conditions). Finally, note that the pulsation velocity, $W_b(z)$, is identical to $\Theta_b(z)$ in the case of horizontal high-frequency vibrations along x.

The exact solution to the problem is obtained by solving the coupled differential equations (4)-(5) analytically. By noting

$$N_1(Gs) = \sinh \frac{Gs^{1/4}}{2\sqrt{2}} \cos \frac{Gs^{1/4}}{2\sqrt{2}}, \quad N_2(Gs) = \cosh \frac{Gs^{1/4}}{2\sqrt{2}} \sin \frac{Gs^{1/4}}{2\sqrt{2}},$$

and

$$\begin{aligned} U_F(z, Gs) &= N_1(Gs) \cosh \frac{Gs^{1/4} z}{\sqrt{2}} \sin \frac{Gs^{1/4} z}{\sqrt{2}} - N_2(Gs) \sinh \frac{Gs^{1/4} z}{\sqrt{2}} \cos \frac{Gs^{1/4} z}{\sqrt{2}}, \\ \Theta_F(z, Gs) &= N_1(Gs) \sinh \frac{Gs^{1/4} z}{\sqrt{2}} \cos \frac{Gs^{1/4} z}{\sqrt{2}} + N_2(Gs) \cosh \frac{Gs^{1/4} z}{\sqrt{2}} \sin \frac{Gs^{1/4} z}{\sqrt{2}}, \end{aligned}$$

$U_b(z)$ and $\Theta_b(z)$ may be expressed as follows:

$$U_b(z) = \frac{\sqrt{2}\, Gr}{Gs^{3/4} D_{I-BC}(Gs)}\ U_F(z, Gs), \tag{6a}$$

$$\Theta_b(z) = W_b(z) = \frac{GrPr}{Gs}\, z - \frac{\sqrt{2}\, GrPr}{Gs^{5/4} D_{I-BC}(Gs)}\ \Theta_F(z, Gs), \tag{6b}$$

with

$$D_{I-BC}(Gs) = \sinh \frac{Gs^{1/4}}{2\sqrt{2}} \cosh \frac{Gs^{1/4}}{2\sqrt{2}} + \sin \frac{Gs^{1/4}}{2\sqrt{2}} \cos \frac{Gs^{1/4}}{2\sqrt{2}}$$

in the case with thermally insulating boundaries, and

$$U_b(z) = \frac{Gr}{2\,Gs^{1/2} D_{C-BC}(Gs)}\ U_F(z, Gs), \tag{7a}$$

$$\Theta_b(z) = W_b(z) = \frac{GrPr}{Gs}\,z - \frac{GrPr}{2\,Gs\,D_{C-BC}(Gs)}\ \Theta_F(z, Gs), \tag{7b}$$

with

$$D_{C-BC}(Gs) = N_1(Gs)^2 + N_2(Gs)^2$$

in the case with thermally conducting boundaries. Note that similar solutions have been given by Gershuni and Lyubimov (1998), Birikh and Katanova (1998), for example, in the case of thermally conducting walls, or even by Lappa (2012) in the general situation of tilted vibrations.

Finally, it is interesting to evaluate the asymptotic expressions of the velocity profiles for $Gs \to 0$. The series expansion of the expressions (6a) and (7a) is:

$$U_b(z) = Gr\left[\left(\frac{z^3}{6} - \frac{z}{24}\right) - Q(z)Gs\right] + \mathcal{O}\left(Gs^2\right) \tag{8}$$

with

$$Q(z) = \frac{z^7}{5040} - \frac{z^5}{2880} + \frac{z^3}{2304} - \frac{29z}{322560} \tag{9}$$

in the case with thermally insulating boundaries, and

$$Q(z) = \frac{z^7}{5040} - \frac{z^5}{2880} + \frac{7z^3}{34560} - \frac{31z}{967680} \tag{10}$$

in the case with thermally conducting boundaries.

From the expression (8), we can also show that, regardless of the thermal boundary conditions type, the limit of $U_b(z)$ when $Gs \to 0$ (i.e., without vibrations) is the well-known cubic Hadley profile obtained, for example, by Hart (1972):

$$U_h(z) = \frac{Gr}{6}\left(z^3 - \frac{z}{4}\right). \tag{11}$$

If the Hadley profile for the velocity (Eq. (11)) is independent of the thermal boundary conditions, this is not the case for the temperature profile, which is given by the following expressions:

$$\Theta_h(z) = GrPr\left(\frac{z^5}{120} - \frac{z^3}{144} + \frac{z}{384}\right) \tag{12}$$

in the case with thermally insulating boundaries, and

$$\Theta_h(z) = GrPr\left(\frac{z^5}{120} - \frac{z^3}{144} + \frac{z}{5760}\right) \tag{13}$$

in the case with thermally conducting boundaries. These reference profiles, obtained for $Gs = 0$, are given in figure 2 as solid black lines with stars.

Equation (8) also indicates that, when high-frequency vibrations are applied, the departure of the velocity from the Hadley profile occurs proportionally to Gs.

To understand the effect of high-frequency horizontal vibrations on the basic flow, a parametric study is performed by considering different values of the Gershuni number Gs and the Prandtl number Pr for both thermally insulating and conducting walls. The velocity $u_b(z) = U_b(z)/Gr$ and the temperature $\theta_b(z) = \Theta_b(z)/(Gr\,Pr)$ profiles for four values $\{0, 100, 500, 1000\}$ of Gs are shown in figure 2 for thermally insulating (Figs. 2a & 2c) and thermally conducting walls (Figs. 2b & 2d). We observe that the flow intensity (Figs. 2a & 2b) decreases gradually when the Gershuni number increases. Similarly, the temperature profiles (Figs. 2c & 2d) have a reduced intensity as a result of the damping of the velocity intensity for both types of thermal boundary conditions. This indicates that applying high-frequency vibrations in the longitudinal direction will dampen the basic steady flow and, therefore, will have consequences on the instabilities that are expected to set in.

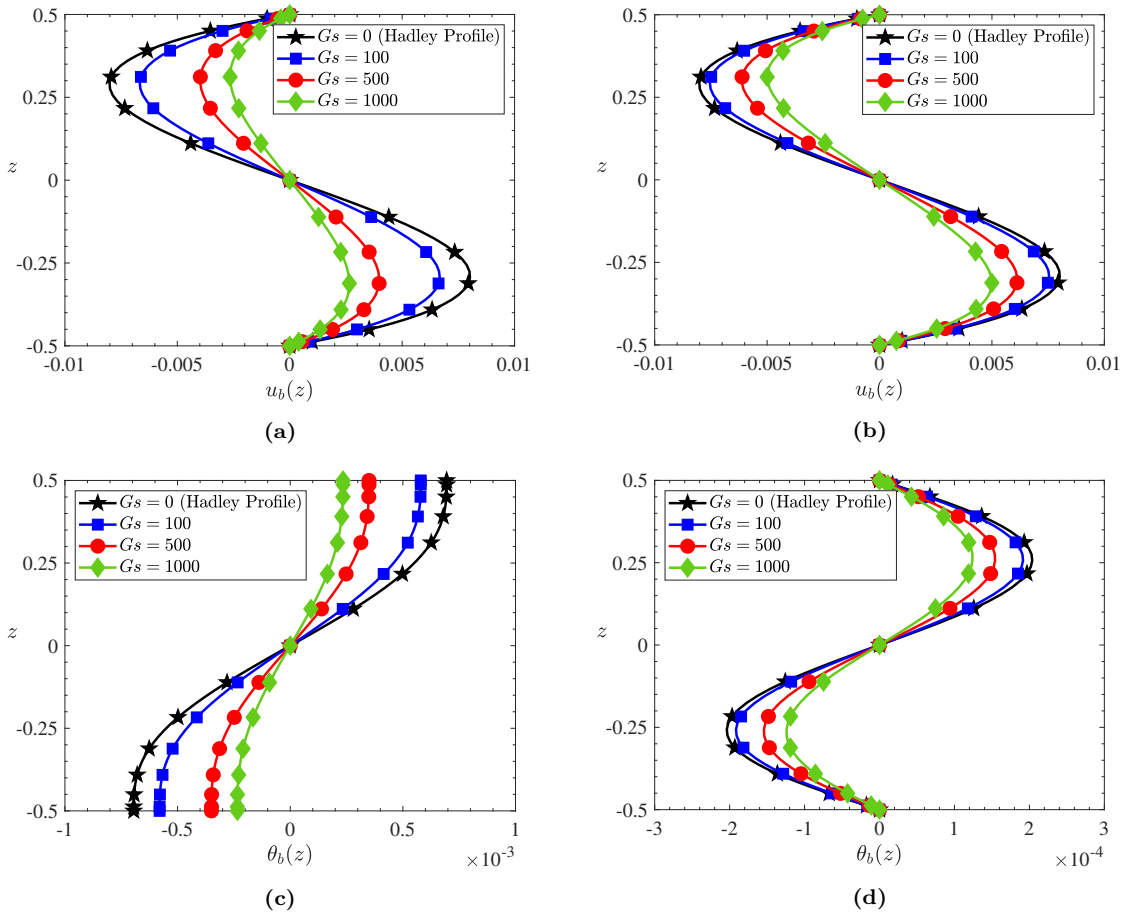

Figure 2: Vertical basic steady-state profiles of the velocity $u_b(z) = U_b(z)/Gr$ and the temperature $\theta_b(z) = \Theta_b(z)/(Gr\,Pr)$ for different Gs numbers at $Pr = 0.1$ and $Gr = 1000$ in the cases of insulating walls (a and c) and conducting walls (b and d).

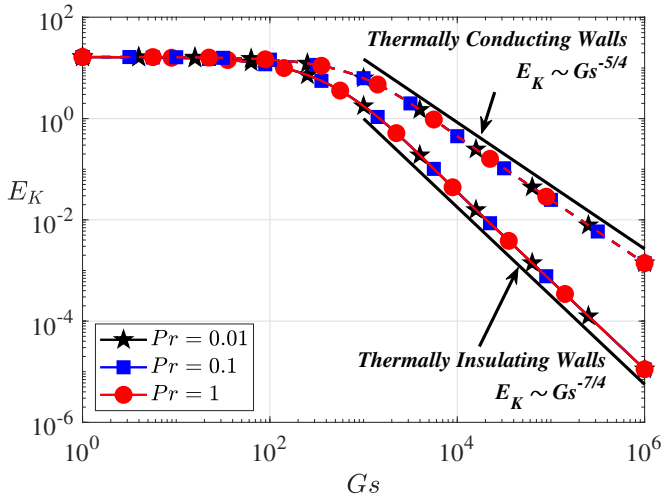

Figure 3: Evolution of the basic flow averaged kinetic energy E_K as a function of Gs for different Prandtl numbers at $Gr = 1000$. The curves corresponding to thermally insulating/conducting walls are plotted using solid/dashed lines.

It is also worthwhile to highlight the effects of the Prandtl number and the thermal boundary conditions when high-frequency vibrations are applied. The average kinetic energy, $E_K = (1/2)\int_{-1/2}^{1/2} U_b^2\, dz$, for three values $\{0.01, 0.1, 1\}$ of Pr are shown in figure 3 using solid lines for the curves of the thermally insulating walls and dashed lines for the curves of the thermally conducting walls. At $Gs = 0$, this quantity is the same in all cases as a single Hadley cubic profile describes the flow. When Gs increases, the flow intensity is slightly damped for low and moderate Gs, say up to $Gs = 10^3$. However, when Gs increases further, E_K undergoes a phase of rapid decay with Gs, more efficiently in the case of insulating walls with a $Gs^{-7/4}$ law than in the case of conducting walls with only a $Gs^{-5/4}$ law. Consequently,

the velocity will decrease more rapidly in the case of thermally insulating walls, with a law of the type $U_{I-BC} \sim Gs^{-7/8}$, compared to a law $U_{C-BC} \sim Gs^{-5/8}$ obtained in the case of conducting walls. Moreover, from this figure (Fig. 3), we can deduce that the decay of the flow depends only on the Gershuni number and the boundary conditions, independently of the Prandtl number, as predicted by the analytic solution given above (Eqs. (6a) & (7a)).

Finally, a qualitative analysis of the shape of the steady-state profiles shown in figure 2 allows us to observe the inflectional character of the velocity profile, the thermal stratification of the temperature profiles, and, in the particular situation of thermally conducting boundaries, an unstable stratification in the regions near the walls. These types of profiles are favorable to developing hydrodynamic instabilities of different origins, such as shear and oscillatory modes, due to the inflectional velocity profile and the equilibrium between the stable temperature stratification and the inertia of the fluid particles, respectively. Finally, thermal instabilities of the Rayleigh-Bénard type are likely to develop in the regions of unstable stratification that occur in the case of thermally conducting walls.

In the following sections, we present a detailed study concerning the linear stability of the buoyancy-driven flow occurring between two infinite horizontal walls and submitted to high-frequency horizontal vibrations. The effects of Prandtl number and thermal boundary conditions are investigated, together with an energy analysis at the thresholds to identify the instability triggering mechanism in each situation.

3 Linearized equations and numerical techniques

The stability of the basic steady flow presented above is performed in the framework of linear stability analysis. Indeed, the general solution of the physical problem is expressed as $\vec{U} = \vec{U}_b + \vec{u}$, $\vec{W} = \vec{W}_b + \vec{w}$, $T = T_b(x,z) + \theta$ and $P = P_b + p$ where $\{\vec{u}(u_x, u_y, u_z), \theta, p, \vec{w}(w_x, w_y, w_z)\}$ are infinitesimal disturbances. Then, by introducing this solution in the system of equations (1a)-(1e) and after linearization around the basic state, we obtain the governing system for these disturbances:

$$\frac{\partial \vec{u}}{\partial t} + (\vec{u}.\vec{\nabla})\vec{U}_b + (\vec{U}_b.\vec{\nabla})\vec{u} = -\vec{\nabla}p + \Delta\vec{u} + Gr\,\theta\vec{e}_z + \frac{Gs}{Pr}\left[(\vec{W}_b.\vec{e}_x)\,\vec{\nabla}\theta + (\vec{w}.\vec{e}_x)\,\vec{\nabla}T_b\right], \tag{14a}$$

$$\frac{\partial \theta}{\partial t} + (\vec{U}_b.\vec{\nabla})\theta + (\vec{u}.\vec{\nabla})T_b = \frac{1}{Pr}\Delta\theta, \tag{14b}$$

$$\vec{\nabla} \times \vec{w} = \vec{\nabla}\theta \times \vec{e}_x, \tag{14c}$$

$$\vec{\nabla} \cdot \vec{u} = 0, \tag{14d}$$

$$\vec{\nabla} \cdot \vec{w} = 0. \tag{14e}$$

Here, note that taking the curl of equation (14c) and using (14e) give a Poisson equation for the field of pulsation velocity $\vec{w}$,

$$\Delta\vec{w} = \Delta\theta\vec{e}_x - (\vec{e}_x \cdot \vec{\nabla})\vec{\nabla}\theta. \tag{15}$$

In the case of cavities with infinite horizontal dimensions, the perturbations can be decomposed into Fourier normal eigenmodes of the following form:

$$\{\vec{u}, \theta, p, \vec{w}\} = \left\{\vec{\hat{u}}(z), \hat{\theta}(z), \hat{p}(z), \vec{\hat{w}}(z)\right\} e^{st+i(hx+ky)}, \tag{16}$$

where h and k are real wave numbers in the longitudinal, x, and transverse, y, directions, and $s = \sigma + i\omega$ is a complex eigenvalue for which σ represents the growth rate and ω the oscillation frequency of the instability. By substituting this form of perturbation into the previous set of equations, a generalized eigenvalue problem is obtained: $L\vec{X} = (\sigma + i\omega)\,M\vec{X}$, where $\vec{X} = \left\{\vec{\hat{u}}(z), \hat{\theta}(z), \hat{p}(z), \vec{\hat{w}}(z)\right\}^T$, L is a linear operator which depends on h, k, Pr, Gr, and Gs, and M is a constant linear operator. In such a case, only boundary conditions at $z = \pm 1/2$ are needed to solve this eigenvalue problem. They are given by $\hat{u}_x(\pm 1/2) = \hat{u}_y(\pm 1/2) = \hat{u}_z(\pm 1/2) = 0$ and $\hat{\theta}(\pm 1/2) = 0$ for perfectly conducting walls or $d\hat{\theta}/dz(\pm 1/2) = 0$ for perfectly insulating walls. The boundary conditions on the pulsation velocity perturbation are deduced from the expression (14c) and the non-penetration condition $\hat{w}_z(\pm 1/2) = 0$, namely, $d\hat{w}_x/dz(\pm 1/2) = 0$ and $d\hat{w}_y/dz(\pm 1/2) = 0$ for perfectly insulating walls, and $d\hat{w}_x/dz(\pm 1/2) = d\hat{\theta}/dz(\pm 1/2)$ and $d\hat{w}_y/dz(\pm 1/2) = 0$ for perfectly conducting walls.

A numerical code based on the spectral collocation method on Gauss-Lobatto-Chebyshev points has been used to solve this generalized eigenvalue problem and accurately determine the thresholds and their characteristics. From the marginal thresholds $Gr_0(Pr, Gs, h, k)$ for which the largest eigenvalue has a real part equal to zero, the critical Grashof number Gr_c is obtained after minimization along the wave numbers h and k, i.e., $Gr_c = \min_{(h,k)\in\mathcal{R}^2} Gr_0(Pr, Gs, h, k)$.

The minimization procedure is performed using a simplex method developed by Nelder and Mead (1965). It is a method that attempts to find the local minima of a continuous function in a multidimensional space by leveraging the concept of a simplex, a polytope of $N+1$ vertices in a N dimensional space. In our study, the simplex formed for a two variables (h and k) function is a triangle for which the values of the function at its three vertices are compared. Initially starting from such a triangle, it undergoes simple transformations during iterations: the worst vertex (for which the value of the function is the largest one) is rejected and replaced with a new vertex as described by Nelder and Mead (1965). At each iteration, the triangle deforms, moves in the wave numbers space, and reduces progressively until its vertices approach a point where the function is at its minimum. For more details on the method, its properties, and its practical use, the reader can consult Lagarias et al. (1998) and Mathews and Fink (1999). Finally, the critical modes will be found to be transverse ($h \neq 0$, $k = 0$) or longitudinal ($h = 0$, $k \neq 0$), and either stationary or oscillatory, depending on whether the imaginary part of the corresponding eigenvalue is zero or nonzero, respectively.

4 Energy budgets

The physical mechanisms involved in the triggering of the instabilities can be determined by energy budgets at the thresholds. These budgets will concern the fluctuating kinetic energy and the thermal energy, denoted as K and E, respectively. Note that the methodology adopted in this work is the same as that followed by Kaddeche et al. (2003) and Medelfef et al. (2017), and only the final integral quantities are provided in this section.

The fluctuating kinetic energy K is obtained after multiplying the disturbance $\vec{u}$ (the eigenvector corresponding to the most unstable eigenvalue) by its complex conjugate $\vec{u}^*$ and integrating over the vertical direction z. The equation governing the rate of change of K is given by

$$\mathcal{R}e\left(\frac{\partial K}{\partial t}\right) = \sigma \int_z \vec{u}\cdot\vec{u}^* dz = K_s + K_b + K_d + K_v, \tag{17}$$

where

$$K_s = -\mathcal{R}e\left\{\int_z \left(u_z\, u_x^* \frac{dU_b}{dz}\right) dz\right\}$$

is the production of fluctuating kinetic energy by shear of the basic state velocity,

$$K_b = \mathcal{R}e\left\{Gr \int_z (u_z^*\,\theta)\, dz\right\}$$

is the buoyancy contribution to the fluctuating kinetic energy,

$$K_d = \mathcal{R}e\left\{\int_z (\vec{u}^*\cdot\Delta\vec{u})\, dz\right\}$$

is the viscous dissipation of fluctuating kinetic energy and, finally,

$$K_v = \mathcal{R}e\left\{\frac{Gs}{Pr}\int_z \left(\vec{u}^*\cdot\left[W_b\vec{\nabla}\theta + w_x\vec{\nabla}T_b\right]\right) dz\right\}$$

represents the contribution of the horizontal high-frequency vibrations to the fluctuating kinetic energy budget. Using equations (2) and (14d) while integrating by parts, this term can be expressed as the sum of two contributions K_{v1} and K_{v2} such that

$$K_{v1} = \mathcal{R}e\left\{\frac{Gs}{Pr}\int_z \left(u_z^*\,(w_x-\theta)\,\frac{\partial\Theta_b}{\partial z}\right) dz\right\},$$

and

$$K_{v2} = \mathcal{R}e\left\{\frac{Gs}{Pr}\int_z (u_x^*\, w_x)\, dz\right\},$$

which are related to the vertical and the imposed horizontal gradients of the basic state temperature, respectively. Furthermore, for three-dimensional longitudinal modes, equation (14c) gives $w_x = \theta$, so that the first term K_{v1} vanishes, and hence $K_v = K_{v2}$ for these instabilities.

Finally, note that the contribution of the pressure term

$$K_p = -\mathcal{R}e\left\{\int_z \left(\vec{u}^*\cdot\vec{\nabla}p\right) dz\right\}$$

is zero and therefore has not been included in equation (17).

The fluctuating thermal energy E is obtained after multiplying the disturbance θ by its complex conjugate θ^* and integrating over the vertical direction z. The equation governing the rate of change of E is given by

$$\mathcal{R}e\left(\frac{\partial E}{\partial t}\right) = \sigma \int_z \theta \cdot \theta^* dz = E_x + E_z + E_d, \tag{18}$$

where

$$E_x = -\mathcal{R}e\left\{\int_z (\theta^*\, u_x)\, dz\right\}$$

is a production term related to the longitudinal gradient of temperature,

$$E_z = -\mathcal{R}e\left\{\int_z \left(\theta^*\, u_z\, \frac{d\Theta_b}{dz}\right) dz\right\}$$

represents a production term related to the vertical gradient of temperature, and, finally,

$$E_d = \mathcal{R}e\left\{\frac{1}{Pr}\int_z (\theta^* \cdot \Delta\theta)\, dz\right\}$$

is a dissipation term connected to heat diffusion.

The disturbances associated with the critical eigenvectors being defined to within a multiplicative constant, we normalize the integral quantities in the kinetic energy (thermal) budget with the viscous (thermal) dissipation, more precisely $|K_d| = -K_d$ ($|E_d| = -E_d$), using the fact that K_d (E_d) is stabilizing by nature and thus a negative term. Moreover, at the threshold, the critical eigenvector is associated with an eigenvalue of zero real part, i.e., $\sigma = 0$. This implies that equations (17) and (18) are both equal to zero at marginal stability. Applying the normalization to equations (17) and (18), we get the following equations involving normalized energy terms at threshold:

$$K'_s + K'_b + K'_{v1} + K'_{v2} = 1, \tag{19a}$$
$$E'_x + E'_z = 1. \tag{19b}$$

Finally, note that positive (negative) energy terms are destabilizing (stabilizing) in these normalized equations (19a) and (19b).

5 Stability results

Before we investigate the effect of horizontal high-frequency vibrations on the stability of Hadley flow, it is worthwhile to recall the different instabilities that develop in the static situation (without vibrations) of the cubic Hadley profile, i.e., for $Gs = 0$. Table 1 gives the dominant primary instabilities obtained for $Pr \leqslant 1$ in a side-heated infinite fluid layer bounded by two horizontal rigid walls, in the case without vibrations. The critical characteristics of these instabilities are given for selected values of Pr and the Pr domains where each instability mode is the most dangerous are finally mentioned. All this information agrees very well with the results presented in the previous studies. In addition to the instabilities mentioned in Tab. 1, Gershuni et al. (1992) pointed out the existence of another instability mode of thermal origin, which never becomes dominant in the classical case without vibrations. This mode develops near the horizontal walls as two-dimensional oscillatory transverse rolls in the case of thermally conducting boundaries. As will be shown in this paper, it may become dominant when high-frequency vibrations are applied.

5.1 General effect of the vibrations on the different instabilities

The action of high-frequency vibrations on the different instabilities is shown through critical stability curves in figure 4. These curves give the evolution of the critical Grashof number Gr_c as a function of the Prandtl number Pr for five values $\{0, 500, 1000, 1500, 2000\}$ of Gs with either thermally insulating (Fig. 4a) or thermally conducting (Fig. 4b) walls.

Several observations are drawn from this figure (Fig. 4). First, all the critical stability curves are shifted to higher values when Gs increases, which indicates a global stabilizing action of high-frequency vibrations on the buoyancy-driven flow. In addition, for the two-dimensional stationary transverse and three-dimensional oscillatory longitudinal modes developing at low Prandtl numbers, the curves evolve similarly regardless of the imposed thermal boundary conditions. Indeed, the thresholds corresponding

Table 1: Most dominant instabilities in the range $Pr \leqslant 1$, along with their critical characteristics for selected values of Pr, for a side-heated infinite layer in the case without vibrations, i.e., for $Gs = 0$. STM stands for Stationary Transverse Mode, whereas OLM and SLM refer to Oscillatory and Stationary Longitudinal Modes, respectively. For each instability, the range of Pr where it is dominant is also indicated.

Characteristics	STM (Shear instability, 2D)	OLM (Oscillatory instability, 3D)	SLM (Shear or thermal instability, 3D)
Thermally insulating walls			
Pr	0.01	0.1	1
Gr_c	8165.19	7342.14	694357.73
h_c	2.68	0	0
k_c	0	1.02	3.25
ω_c	0	38.96	0
Range of Pr	$Pr \leqslant 0.033$	$0.033 \leqslant Pr \leqslant 0.207$	$Pr \geqslant 0.207$
Thermally conducting walls			
Pr	0.01	0.1	1
Gr_c	8076.92	20466.79	12993.47
h_c	2.68	0	0
k_c	0	2.01	8.27
ω_c	0	126.47	0
Range of Pr	$Pr \leqslant 0.137$	$0.137 \leqslant Pr \leqslant 0.447$	$Pr \geqslant 0.447$

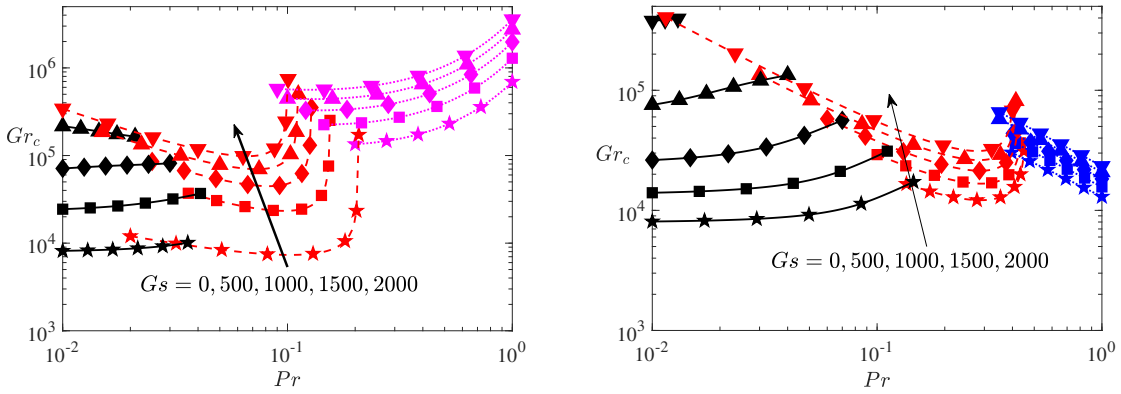

Figure 4: Instability thresholds Gr_c as a function of Pr for the main modes at $Gs = 0$ (stars), 500 (squares), 1000 (lozenges), 1500 (up-pointing triangles), and 2000 (down-pointing triangles) for thermally insulating walls (a) and thermally conducting walls (b). Stationary transverse modes (STM) curves are plotted using solid black lines, oscillatory longitudinal modes (OLM) curves are given as red dashed lines, and stationary longitudinal modes (SLM) are shown as magenta dotted lines for the insulating walls (shear instability) and blue dotted lines for the conducting walls (thermal instability).

to the stationary two-dimensional transverse mode are flat at very low Pr (asymptotic limit for $Pr \to 0$ for these shear instabilities), have then slow variation with Pr, and eventually increase at moderate Pr, rather outside their domain of predominance shown here. In contrast, the oscillatory three-dimensional longitudinal mode undergoes a decrease in the critical thresholds with the initial increase of Pr, followed by a steep growth when Pr is further increased. Moreover, we can also see that the stationary transverse mode is more efficiently stabilized than the oscillatory longitudinal mode.

As for the stationary three-dimensional longitudinal modes developing at higher Pr values, the variation of their thresholds with Pr depends on the boundary conditions: the critical curves increase with Pr in the case of thermally insulating walls, whereas they decrease in the case of conducting walls. This is mainly because these stationary longitudinal modes trace their origins to different physical mechanisms. Indeed, for thermally insulating walls, the longitudinal mode is triggered by shear near the wall (shear instability, magenta curves in figure 4a) while, for thermally conducting boundaries, it is caused by buoyancy, as a consequence of the unstable temperature stratification near the walls (thermal instability, blue curves in figure 4b). Nevertheless, both modes develop as three-dimensional stationary longitudinal rolls in the wall regions.

Finally, Fig. 4 shows that the intersection points between the critical stability curves related to each

mode move in the Pr range when the cavity is subjected to high-frequency vibrations with increasing Gs, thus modifying the predominance domain of the corresponding instabilities as a function of Gs, Pr, and the thermal boundary conditions. The evolution of these intersection points is more precisely shown as a mode-map in the (Gs, Pr) space in Fig. 5a (thermally insulating walls) and Fig. 5b (thermally conducting walls). Five instability zones are identified depending on the thermal boundary conditions. Zones I and II, which represent the regions where the stationary transverse and oscillatory longitudinal modes are dominant, respectively, are present in both cases of thermal boundary conditions. Zone III represents the region where a stationary longitudinal mode of dynamical origin is dominant for thermally insulating walls. In contrast, zones IV and V represent the regions where stationary longitudinal and oscillatory transverse modes of thermal origin dominate for thermally conducting walls.

The first intersection point encountered as the Prandtl number Pr is increased (Fig. 5) corresponds to the transition between the stationary transverse mode (zone I) and the oscillatory longitudinal mode (zone II). From the evolution of this point, we see that the stationary transverse mode, dominant at very low Pr numbers, appears in a tighter Pr range as Gs increases, indicating the disappearance of this mode in favor of the oscillatory instability, whose area of predominance widens towards small Pr numbers. This effect is well marked for both boundary conditions, and above rather moderate values of Gs (around 1700 for I-BC and 2100 for C-BC), the stationary transverse mode is no more dominant in the whole range $Pr \geqslant 0.01$.

The second intersection point indicates the transition between the oscillatory longitudinal mode (zone II) and the stationary longitudinal modes of either dynamical (zone III) or thermal (zone IV) origin. We see that this point also moves towards smaller Pr values as Gs is increased, but in a moderate way compared with the first intersection point. This effect is more pronounced in the case of thermally insulating boundaries in comparison with the case of thermally conducting boundaries. Indeed, for insulating walls (Fig. 5a), the Pr values above which the stationary longitudinal mode dominates the oscillatory mode change approximately from 0.2 for $Gs = 0$ to 0.1 for $Gs = 2000$, whereas, for conducting walls (Fig. 5b), these Pr values only change from 0.45 to 0.4.

Finally, in the case of conducting walls (Fig. 5b), our stability calculations reveal the existence of a third intersection point starting at $Gs \approx 1100$ for $Pr = 1$, beyond which the three-dimensional stationary longitudinal mode of thermal origin (zone IV) is no longer dominant. Indeed, a two-dimensional oscillatory transverse mode (zone V) becomes the most dangerous, with a predominance zone that widens as the Gershuni number Gs increases. This oscillatory transverse mode is the one identified by Gershuni et al. (1992). This mode is never dominant in the absence of vibrations and was then not mentioned in figure 4b.

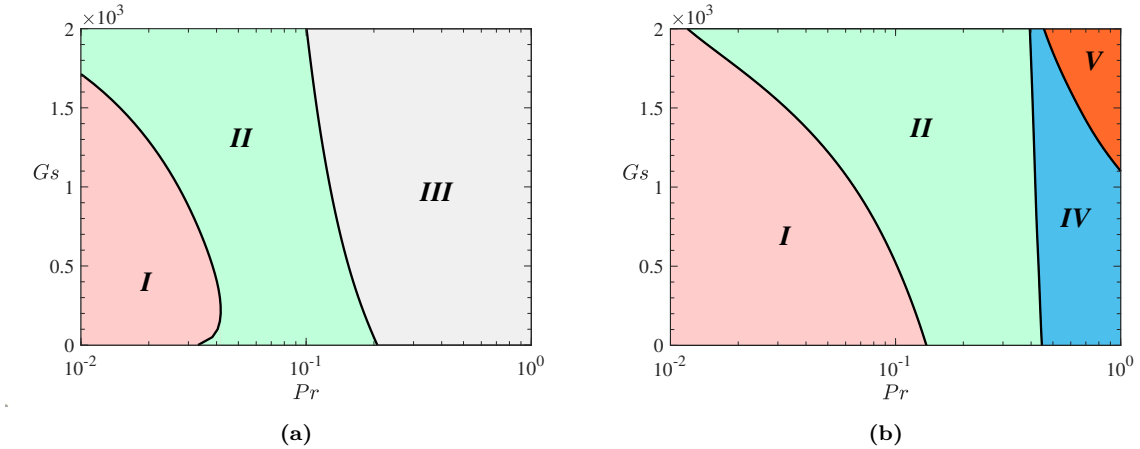

Figure 5: Instability map in the (Gs, Pr) space showing the extent of the zones where the different modes are dominant in the case of thermally insulating walls (a) and thermally conducting walls (b). Zones I and II concern the stationary transverse and the oscillatory longitudinal modes, zones III and IV the stationary modes with dynamical and thermal origins, respectively, and zone V refers to the oscillatory transverse mode.

In what follows, we will deepen our study of the vibration influence on the different instabilities for three Prandtl numbers well related to the predominance zones, namely, $Pr = 0.01$, 0.1, and 1. The stationary transverse shear mode and the oscillatory longitudinal mode are studied for $Pr = 0.01$ and $Pr = 0.1$, respectively, whereas the stationary longitudinal (shear or thermal) modes and the oscillatory transverse thermal mode are studied for $Pr = 1$.

5.2 Stationary transverse shear mode (*Pr=0.01*)

The stabilizing effect of the high-frequency vibrations on the 2D stationary transverse shear mode is considered here for the two types of thermal boundary conditions at $Pr = 0.01$. In the case without vibrations (i.e., $Gs = 0$), this shear instability is of dynamical origin and develops at very low Prandtl numbers. Buoyancy does not play a significant role in this instability, as indicated by the weak effect of the boundary conditions on the instability critical characteristics. For example, for $Pr = 0.01$, the onset of this instability is $Gr_c = 8165$ (with $h_c = 2.68$) for thermally insulating walls, versus $Gr_c = 8076$ (with $h_c = 2.68$) for thermally conducting walls. The plot of the marginal transverse rolls in terms of streamlines in the longitudinal xz plane, given in figures 6a and 6b, confirms the similarity between the modes obtained with both boundary conditions.

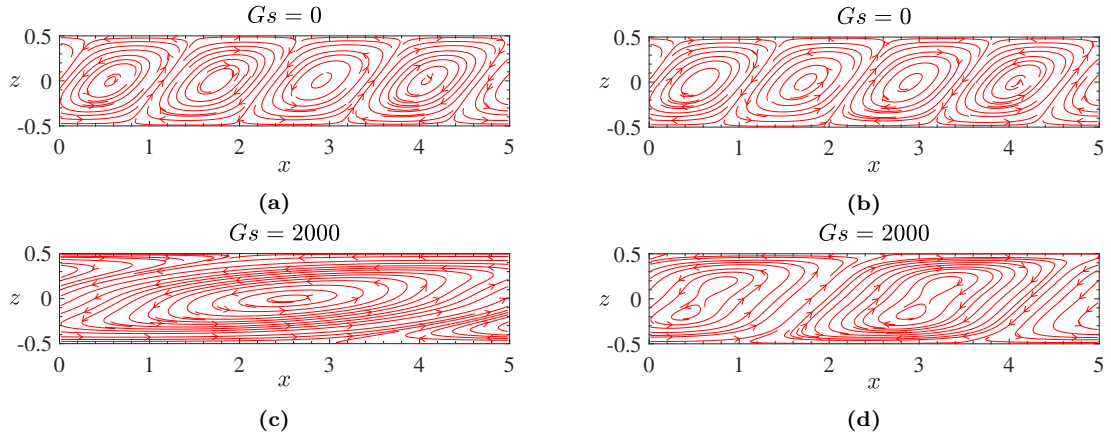

Figure 6: Streamlines corresponding to the stationary transverse rolls (shear instability) in the longitudinal xz plane for insulating walls (left, a & c) and conducting walls (right, b & d) for $Gs = 0$ and 2000 at $Pr = 0.01$.

The variation of the shear instability thresholds Gr_c/Gr_{c0} (where the subscript 0 refers to the case without vibrations, $Gs = 0$) with Gs is given in figure 7a for $Pr = 0.01$ and both thermally insulating (solid line) and conducting (dashed line) walls. As Gs increases, the critical curves corresponding to the two types of thermal boundary conditions increase from 1 to several dozens at $Gs = 2500$, thus corroborating the stabilizing effect observed in the previous section (Fig. 4). However, the critical Grashof number, Gr_c, evolves differently depending on the type of thermal boundary conditions.

In the insulating walls case, the critical threshold Gr_c undergoes a fast exponential growth phase with $Gr_c/Gr_{c0} \approx \exp(0.02\,Gs)$ for $Gs \lesssim 1500$ and then begins a phase of saturation with $Gr_c/Gr_{c0} \approx 110 \exp\left(-3.2 \times 10^6/Gs^2\right)$. In contrast, for conducting walls, we obtain a slower initial growth phase with $Gr_c/Gr_{c0} \approx \exp(0.01\,Gs)$ for $Gs \lesssim 1200$, followed by a faster growth phase with $Gr_c/Gr_{c0} \approx 0.06 \exp(0.03\,Gs)$. As a result of these variations, the initial stabilizing action of the high-frequency vibrations is more pronounced in the case of insulating walls (solid line). This behavior mainly comes from the fact that this shear instability is connected to the velocity profile, which undergoes a faster decay in the case of insulating walls, as can be seen in figure 3 through the kinetic energy of the basic flow. However, due to the further saturation phase in the case of insulating walls and the strong growth in the case of conducting walls, the two critical curves will then cross for $Gs \approx 2000$, so that $(Gr_c)^{\text{C-BC}} < (Gr_c)^{\text{I-BC}}$ before this Gs value and $(Gr_c)^{\text{C-BC}} > (Gr_c)^{\text{I-BC}}$ above. The reason for the saturation phase will be highlighted by energy analyses hereafter. Note that we have difficulties to follow these instability thresholds very far in Gs. For $Pr = 0.01$, limit values are found at $Gs \approx 2700$ and $Gs \approx 3000$ for insulating and conducting walls, respectively.

Information on the size of the marginal rolls is given in figure 7b through the variation of the critical wave number h_c with Gs. h_c globally decreases with the increase of Gs, which indicates that the marginal cells, whose size is given by $\lambda_c = 2\pi/h_c$, become longer under the action of high-frequency vibrations. More precisely, there is a weak initial decrease, up to $Gs \approx 500$, followed by a phase of larger decrease, and an eventual phase of saturation. Both boundary conditions give a similar decrease up to $Gs \approx 1500$, but the decrease is then more pronounced in the case of insulating walls (solid line) where the saturation occurs for slightly larger Gs. The increase of the size of the marginal rolls is illustrated in figure 6, where the marginal transverse rolls in the longitudinal xz plane are given for $Gs = 0$ and 2000 and for both boundary conditions. We see that, for conducting walls, the size of the rolls is approximately doubled when Gs is increased from 0 to 2000 (Figs. 6b & 6d). As expected, the increase is still larger for insulated walls, but the shape of the rolls is also modified, corresponding to an elongated interface between the rolls (Figs. 6a & 6c).

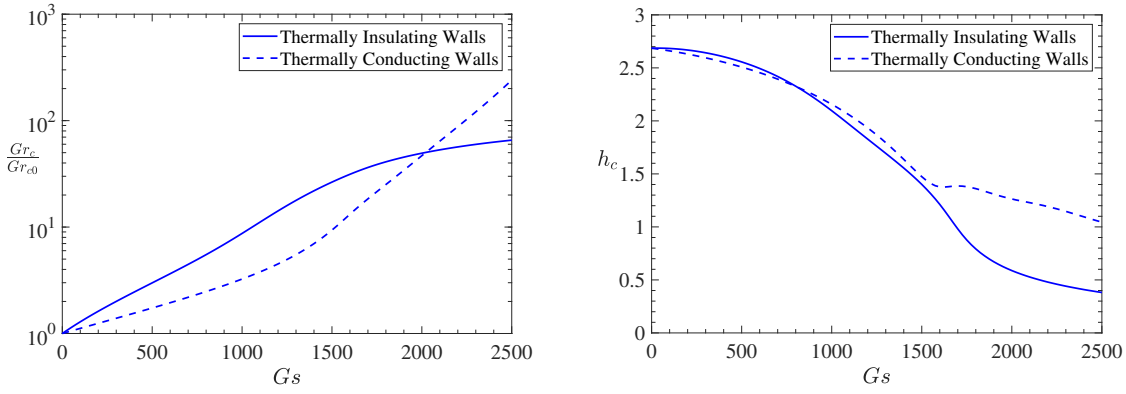

Figure 7: Variation of the critical thresholds Gr_c/Gr_{c0} (a) and critical transverse wave numbers h_c (b) of the stationary transverse modes (shear instability) as a function of the Gershuni number Gs at $Pr = 0.01$.

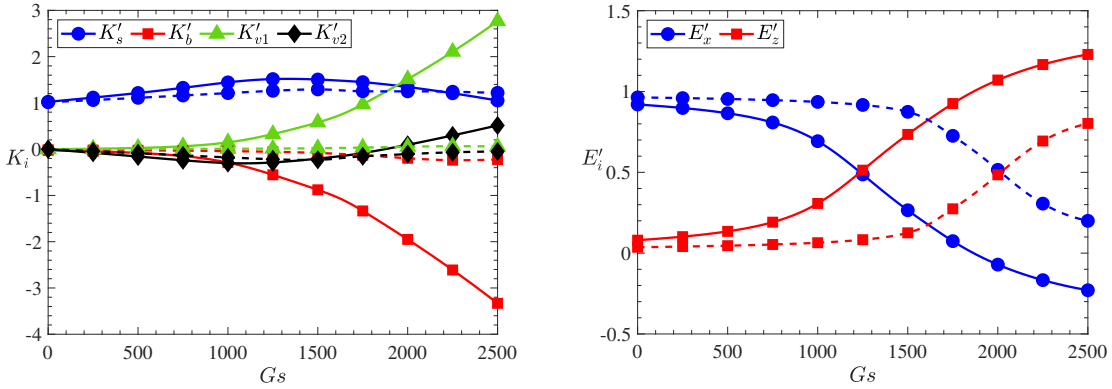

Figure 8: Contributions to the fluctuating kinetic energy (a) and fluctuating thermal energy (b) as a function of the Gershuni number Gs for the stationary transverse modes (shear instability) at $Pr = 0.01$ in the cases of insulating (solid lines) and conducting (dashed lines) walls.

Finally, figure 8 provides more information about the physical mechanisms involved in triggering or inhibiting the instability. For conducting walls (dashed lines), the contributions to the fluctuating kinetic energy related to buoyancy K'_b and vibrations K'_{v1} and K'_{v2} (Fig. 8a) are weak compared to the contribution of shear K'_s, which remains almost constant, close to 1, when Gs is increased. This indicates that shear remains the main destabilizing effect, equilibrating viscous dissipation, and then that the nature of the instability remains rather unchanged when high-frequency vibrations are applied.

In contrast, for insulating walls (solid lines), the dynamics change when high-frequency vibrations are applied. Indeed, the instability remains mainly triggered by shear (K'_s term), with rather weak other effects (buoyancy K'_b and vibrations K'_{v1} and K'_{v2}) for $Gs \lesssim 1000$. Beyond this value, the contribution of the vibration term K'_{v1} becomes clearly destabilizing (almost up to 3), with a fast increase, while the stabilizing buoyancy contribution K'_b increases too (above 3 in absolute value), with a still slightly faster increase. The contribution of the vibration term K'_{v2}, initially slightly stabilizing, becomes also destabilizing, reaching values up to 0.5. All this indicates that the instability, initially triggered by the shear of the basic flow, becomes driven by both shear and high-frequency vibrations, while inhibited by the buoyancy effect. This behavior, well marked for $Gs \gtrsim 1500$, may explain the observed saturation of the marginal stability curve $(Gr_c)^{\text{I-BC}}$ for insulating walls. Note that the strong increase of K'_{v1} and $|K'_b|$ may be related to the product $u_z^* \theta$ involved in their definition.

The thermal energy budget given in figure 8b shows that the fluctuating thermal energy production, initially driven by the term E'_x related to the imposed longitudinal temperature gradient, becomes increasingly driven by the term E'_z related to the vertical temperature gradient when the Gershuni number is increased. This change is delayed in the case of thermally conducting boundaries, starting at $Gs \approx 500$ for insulating walls (solid lines) and at $Gs \approx 1500$ for conducting walls (dashed lines), with the cross-over between the two effects being observed at $Gs \approx 1250$ and 2000, respectively. Note that the definition of E'_z

corresponds to one of the terms involved in K'_{v1}, which may explain their common increased destabilizing influence.

5.3 Oscillatory longitudinal mode (*Pr=0.05-0.1*)

The effect of high-frequency vibrations on the 3D oscillatory mode is further investigated in this section for $Pr = 0.05 - 0.1$. This instability, developing as longitudinal helicoidal rolls, is of mixed thermal and dynamical origin and is dominant for moderate Prandtl numbers in the case without vibrations, i.e., $Gs = 0$ (see Fig. 4). When Gs increases, this instability becomes dominant even for low Prandtl numbers, as shown in figure 4, regardless of the thermal boundary conditions. Nevertheless, the thermal boundary conditions (insulating or conducting) are expected to play a role, in particular by participating in the changes of the basic velocity and temperature profiles given by Eqs. 6 and 7.

For $Pr = 0.1$ and $Gs = 0$, this oscillatory instability develops at either $Gr_c = 7342.14$ (with $k_c = 1.02$ and $\omega_c = 38.96$) for thermally insulating walls or $Gr_c = 20466.79$ (with $k_c = 2.01$ and $\omega_c = 126.47$) for thermally conducting walls. A plot of the marginal longitudinal rolls in terms of streamlines in the transverse yz plane is given in figures 9a and 9b for thermally insulating and conducting walls, respectively. It shows that the size of the marginal rolls is roughly divided by two when switching from insulating walls to conducting walls, indicating thus an infuence of the thermal boundary conditions even without vibrations.

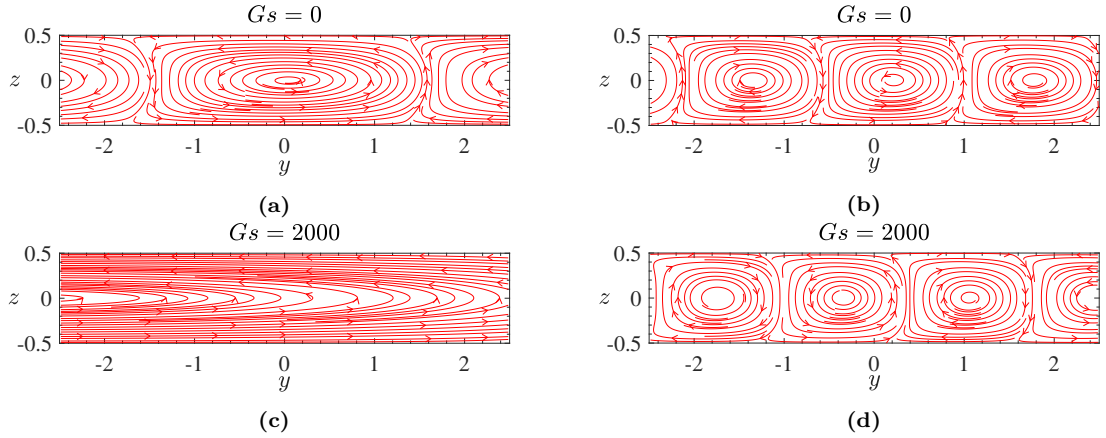

Figure 9: Streamlines corresponding to the oscillatory longitudinal modes in the transverse yz plane for insulating walls (left, a & c) and conducting walls (right, b & d) for $Gs = 0$ and 2000 at $Pr = 0.1$.

Figure 10 gives the critical characteristics of the oscillatory instability as a function of the Gershuni number at $Pr = 0.05$, 0.07, 0.1 for insulating walls (solid lines) and $Pr = 0.1$ for conducting walls (dashed lines). The variations of the instability thresholds Gr_c/Gr_{c0}, given in figure 10a, show a stabilizing effect of the high-frequency vibrations. However, as Gs increases, the marginal curves evolve differently when the boundary conditions and Pr are changed. For conducting walls and $Pr = 0.1$, the evolution of the critical threshold $(Gr_c)^{\text{C-BC}}$ as a function of Gs follows a linear law, $Gr_c/Gr_{c0} \approx 1+0.84\times10^{-3}\,Gs$, which remains valid for Gs values up to 10^5. In contrast, for insulating walls and $Pr = 0.1$, the critical threshold $(Gr_c)^{\text{I-BC}}$ increases very rapidly with Gs, with a growth even tending to ∞ when Gs approaches 2000, indicating the disappearance of this instability close above this value. In order to better understand the very efficient stabilization obtained when high-frequency vibrations are applied in this insulating case, we also give the variation of the thresholds $(Gr_c)^{\text{I-BC}}$ with Gs for $Pr = 0.05$ and 0.07. From these results, we see that the increase of the thresholds can be decomposed in a close to linear initial variation $(Gr_c/Gr_{c0} \approx 1 + 6 \times 10^{-3}\,Gs)$ followed by a strong increase, which occurs for larger Gs when Pr is decreased. An explanation for that is that the action of the high-frequency vibrations has a double effect, an increase of the thresholds (close to linear), but also a displacement of the instability zone towards smaller Pr values. As a consequence, and as shown in figure 4, the limit of the instability zone (corresponding to a very strong increase of the thresholds), which occurs for $Pr \approx 0.2$ without vibration, regularly decreases when Gs is increased and occurs for $Pr \approx 0.1$ when $Gs = 2000$, for example, explaining what is observed for $Pr = 0.1$ in figure 10a. Finally, the conclusion to be drawn from this figure is that high-frequency vibrations have a much more efficient stabilizing effect on the oscillatory longitudinal instability in the case of insulating walls than in the case of conducting walls.

The variation of the critical longitudinal wave number k_c of the instability is given as a function of Gs in figure 10b. This figure shows that k_c behaves differently depending on the thermal boundary conditions. In the case of conducting walls ($Pr = 0.1$), for which the instability threshold grows linearly,

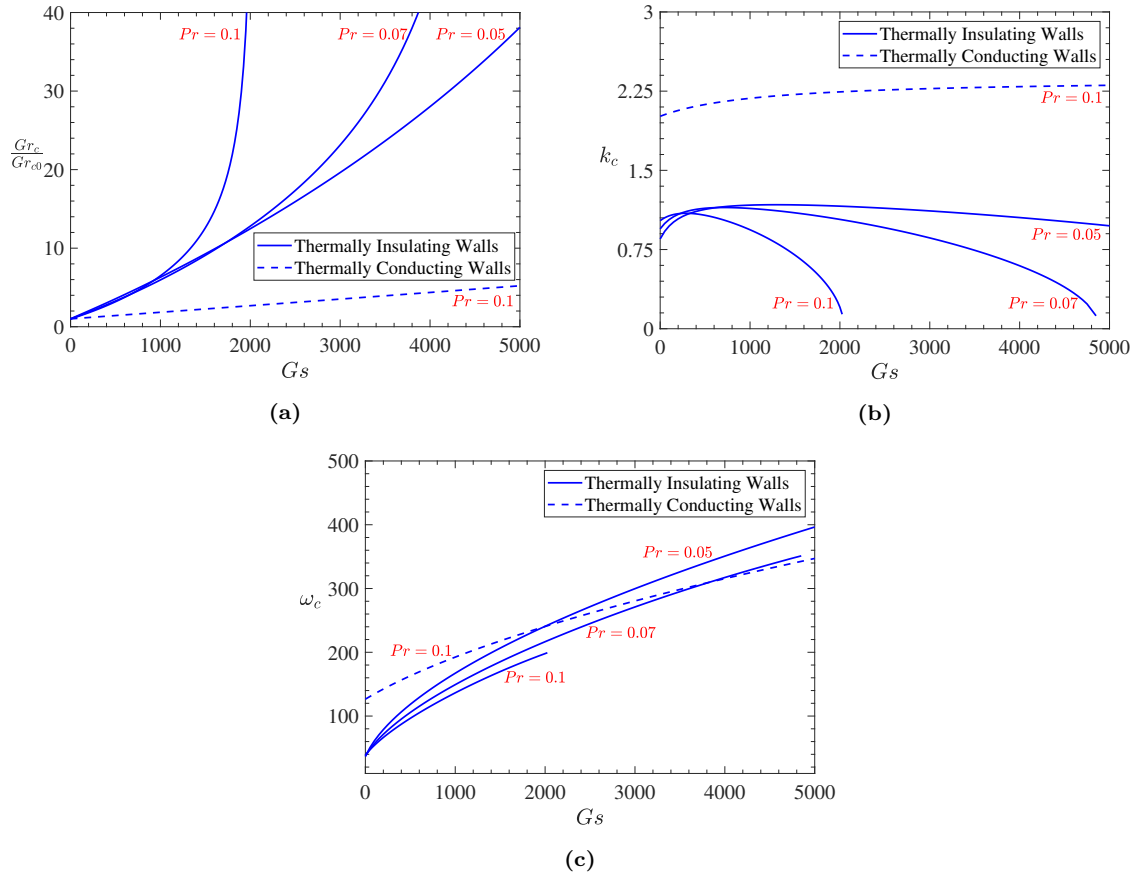

Figure 10: Variation of the critical thresholds Gr_c/Gr_{c0} (a), longitudinal wave numbers k_c (b), and pulsation ω_c (c) of the oscillatory longitudinal modes as a function of the Gershuni number Gs for different Prandtl numbers.

the critical wave number increases slightly for $Gs \lesssim 1000$ and then remains almost constant around $k_c \approx 2.25$ for values of Gs up to 5000. In contrast, in the case of insulating walls, for which the instability threshold eventually increases rapidly with Gs, the initial increase of k_c with Gs is followed by a clear decrease. The precise variation depends on the Prandtl number: the initial increase becomes shorter and less marked, whereas the decrease becomes steeper, when Pr increases from 0.05 to 0.1 (Fig. 10b). To summarize the effect of the vibrations, knowing that the critical wave length is $\lambda_c = 2\pi/k_c$, the cells become slightly shorter in the case of thermally conducting walls, whereas, after an initial shrink, they become longer in the case of thermally insulating walls. These effects are well observed in figure 9.

The critical angular frequency ω_c, given in figure 10c as a function of Gs, evolves in the same way for both insulating and conducting walls when high-frequency vibrations are applied. Indeed, we observe that ω_c increases in a monotonic way with the increase of Gs, the increase being only steeper for insulating walls. Note that the strong modifications of behavior occurring for Gr_c and k_c when Gs is increased in the insulating case are not observed for ω_c. The emergence of a new time scale associated with the oscillation frequency ω_c of the instability induces a new constraint on the validity of the quasi-equilibrium approximation used to derive the model, which is $\Omega \gg \omega_c$, where Ω is the angular frequency of the applied vibrations.

The energy analysis at the threshold of the oscillatory instability is depicted in figures 11a and 11b for the fluctuating kinetic energy and thermal energy, respectively. In these figures, the normalized contributions are given as a function of Gs for insulating walls (solid lines) and conducting walls (dashed lines) at $Pr = 0.1$.

Concerning the kinetic energy, figure 11a shows that the curves corresponding to the different contributions evolve similarly when Gs is increased, with a slightly more accentuated effect in the case of conducting walls than in the case of insulating walls. For $Gs = 0$, the contributions due to shear K'_s and buoyancy K'_b are positive, thus indicating that the oscillatory instability is jointly triggered by shear and buoyancy effects. However, when high-frequency vibrations are applied ($Gs \neq 0$), the shear contribution K'_s becomes increasingly dominant, whereas the buoyancy contribution K'_b, still destabilizing, remains rather constant in comparison. Moreover, the vibration contribution, K'_{v2}, which is zero at $Gs = 0$, has a clear stabilizing effect (negative values), which grows gradually when Gs is increased, almost symmet-

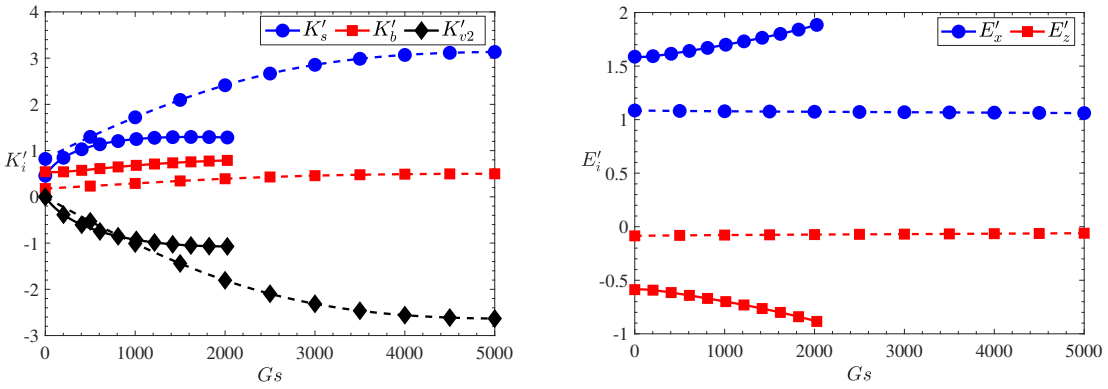

(a) **(b)**

Figure 11: Contributions to the fluctuating kinetic energy (a) and fluctuating thermal energy (b) as a function of the Gershuni number Gs for the oscillatory longitudinal modes at $Pr = 0.1$ in the case of insulating (solid lines) and conducting (dashed lines) walls.

rically with the shear contribution variation. Note that, as indicated in section 4, K'_{v1} is zero in the case of longitudinal modes.

Concerning the thermal energy, Figure 11b shows that, regardless of the thermal boundary conditions, the contribution related to the longitudinal temperature gradient, E'_x, is always positive, thus destabilizing, whereas the contribution related to the vertical temperature gradient, E'_z, is negative, thus stabilizing, and that the changes observed when Gs is increased remain rather moderate. This indicates that the production of fluctuating thermal energy is provided by horizontal heat transport, and that the vertical stratification of the basic steady state given by equations (6b) & (7b) and shown in figures 2c & 2d has a stabilizing influence on this thermal energy analysis.

5.4 Stationary longitudinal mode and oscillatory transverse mode (*Pr=1*)

When the Prandtl number is further increased in the case without vibrations, the favored instabilities develop as three-dimensional stationary longitudinal rolls localized near both the upper and lower horizontal walls (Figs. 12a & 12b) regardless of the thermal boundary conditions. However, in the case of conducting walls, the situation changes when high-frequency vibrations are applied with the emergence of an instability mode having the form of two-dimensional oscillatory transverse rolls (this mode is shown for $Gs = 0$ in Figs. 12c & 12d). Moreover, depending on the thermal boundary conditions, these instabilities are caused by fundamentally different physical mechanisms. Indeed, for thermally insulating walls, the instability is triggered by the shear in the horizontal boundary layer regions (Fig. 12a). In contrast, for thermally conducting walls, the stationary longitudinal (Fig. 12b) and oscillatory transverse (Figs. 12c & 12d) rolls are mainly caused by the unstable thermal stratification occurring near the boundaries. Therefore, in te following, these two types of instability will be considered separately and referred to as *longitudinal shear mode* and *longitudinal or transverse thermal mode*, respectively. The action of high-frequency vibrations on the critical characteristics of these instabilities is studied for $Pr = 1$ and different Gs numbers.

5.4.1 Thermally insulating walls: longitudinal shear mode

We first study the effect of high-frequency vibrations on the longitudinal shear mode for $Pr = 1$. This instability appears as three-dimensional helicoidal rolls developing in the wall regions, as shown in figure 12a through the streamlines in the transverse yz plane. For $Gs = 0$, this instability sets in at $Gr_c = 694\,357$ with a critical wave number $k_c = 3.25$.

Figure 13 shows the variation of the critical thresholds Gr_c/Gr_{c0} and wave number k_c of the longitudinal shear instability as a function of the Gershuni number for $Pr = 1$. As Gs increases, the critical threshold (Fig. 13a) is shifted towards higher Gr_c values, with a variation well approximated by a quadratic law ($Gr_c/Gr_{c0} \approx 1 + 1.79 \times 10^{-3} Gs + 1.45 \times 10^{-7} Gs^2$), but, in fact, close to linear with Gs. Furthermore, the critical wave number k_c (Fig. 13b) increases with Gs, indicating that the marginal rolls become smaller when high-frequency vibrations are applied. Note finally that beyond $Gs \approx 5000$, the instability becomes quite difficult to detect, but its threshold has already been increased by a factor close above 13, indicating the strong stabilization obtained with the high-frequency vibrations.

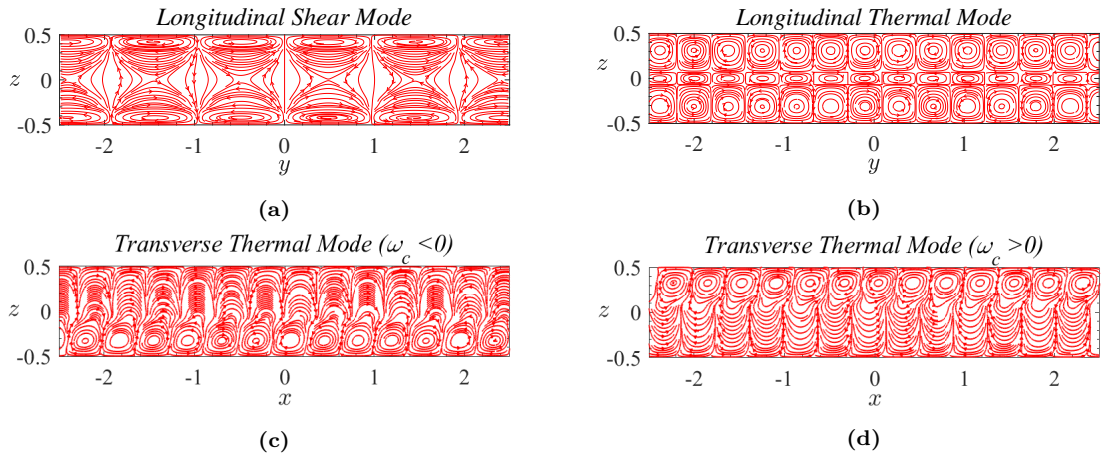

Figure 12: Streamlines corresponding to the different wall modes arising for $Gs = 0$ and $Pr = 1$. The dominant stationary longitudinal modes, due either to shear for thermally insulating walls (a) or to thermal effects for thermally conducting walls (b), are given in the yz plane. The oscillatory transverse modes due to thermal effects (c,d), which are not dominant for $Gs = 0$, are given in the xz plane.

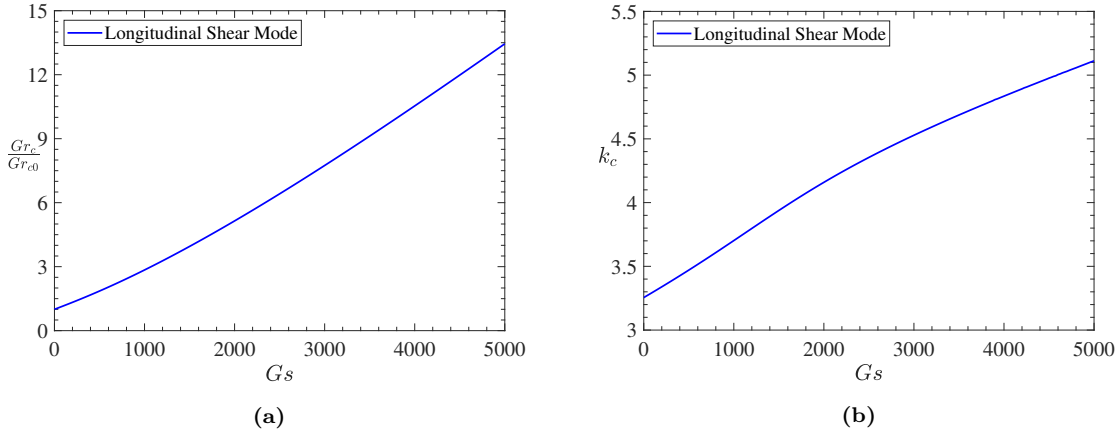

Figure 13: Variation of the critical threshold Gr_c/Gr_{c0} (a) and critical longitudinal wave number k_c (b) of the stationary longitudinal mode (shear instability) as a function of the Gershuni number Gs at $Pr = 1$.

To deepen the origin of this instability, we give the different contributions to the fluctuating kinetic energy K_i' and thermal energy E_i' as a function of the Gershuni number Gs for $Pr = 1$ in figure 14. For the fluctuating kinetic energy, figure 14a shows that all the contributions remain constant as the Gershuni number increases, with a shear term K_s' close to 1, a buoyancy term K_b' remaining very small, and a negligible vibration term K_{v2}'. This indicates that the instability remains of pure shear origin, without influence of the vibration contribution. The strong stabilizing effect observed in figure 13a is then due to the modifications induced in the shear term K_s' by the vibrations, in connection with the strong decrease of the basic flow (Fig. 3), which must be compensated by an increase of the Grashof number to which this basic flow is proportional (Eq. 6a). The fluctuating thermal energy budget (Fig. 14b) is also not influenced by the vibrations, with a destabilizing contribution, E_x', connected with the imposed horizontal gradient of temperature, and a stabilizing contribution, E_z', linked to the vertical gradient of temperature.

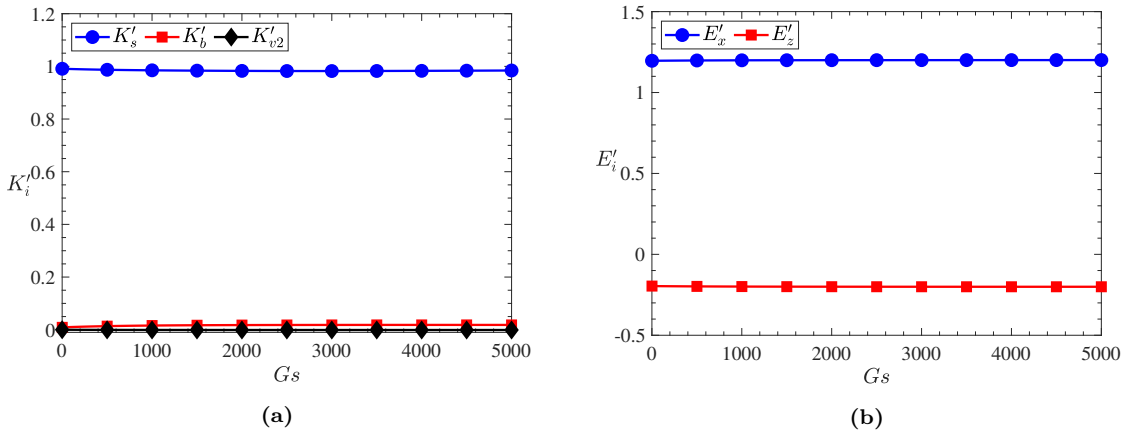

Figure 14: Contributions to the fluctuating kinetic energy (a) and fluctuating thermal energy (b) as a function of the Gershuni number Gs for the shear longitudinal mode at $Pr = 1$.

5.4.2 Thermally conducting walls: longitudinal and transverse thermal modes

We now study the effect of high-frequency vibrations on the thermal modes existing for thermally conducting walls at $Pr = 1$. The first mode is the steady longitudinal Rayleigh mode, dominant at $Gs = 0$, for which the instability appears as three-dimensional helicoidal rolls. These rolls develop in the regions of unstable stratification along the conducting walls, as shown in figure 12b with the plot of streamlines in the transverse yz plane. The onset of this instability is much smaller than that of the longitudinal shear mode obtained for insulating walls. Indeed, for $Gs = 0$, the critical threshold is only $Gr_c = 12\,993$ with a wave number $k_c = 8.27$. The second mode, still of thermal origin but never dominant without vibrations, is an oscillatory transverse mode whose critical threshold at $Gs = 0$ is $Gr_c = 20\,107$ with a critical wave number $h_c = 8.30$. In fact, the resulting instability, associated with pairs of complex conjugate eigenvalues and modes (Figs. 12c & 12d), appears as two traveling waves propagating in opposite directions along x, at the thermally conducting walls.

Figure 15 depicts the variation of the critical characteristics for both of these thermal instabilities as a function of Gs for $Pr = 1$. The critical thresholds are first given in figure 15a. We see the stabilization of the stationary longitudinal mode, with a regular increase of its threshold, which can be well approximated by a quadratic law $Gr_c/Gr_{c0} \approx 1 + 2.70 \times 10^{-3} Gs - 2.27 \times 10^{-7} Gs^2$. In contrast, the oscillatory transverse mode is first slightly destabilized, up to $Gs \approx 604$, before its further stabilization, with an increase of the threshold of the form $Gr_c/Gr_{c0} \approx 0.87 + 1.04 \times 10^{-3} Gs - 3.03 \times 10^{-10} Gs^2$. The stronger increase of the thresholds for the stationary longitudinal mode (dominant at $Gs = 0$) compared with the oscillatory transverse mode, quantified by the larger slope of the linear approximation, will allow the oscillatory transverse mode to become eventually dominant when vibrations are applied.

The change of the dominant thermal mode occurs at the value of Gs corresponding to the crossing of the stability curves. For $Pr = 1$, as shown in figure 15a, the crossing, and then the transition, occurs at $Gs \approx 1100$. This transition point has been calculated for different values of Pr, and is given, in the (Gs, Pr) space, in figure 16. This figure shows that the transition between the stationary longitudinal mode and the oscillatory transverse mode depends on the Prandtl number, occurring earlier, i.e. at lower Gershuni numbers, when Pr is increased. This indicates that the domain where the longitudinal mode is dominant shrinks with the increase of the Prandtl number, allowing the oscillatory transverse mode to become the dominant instability more easily under vibration.

The critical wave numbers h_c and k_c corresponding to the transverse and the longitudinal modes, respectively (Fig. 15b) increase similarly with Gs, but more rapidly for the longitudinal mode wave number k_c, indicating that the marginal rolls become smaller when high-frequency vibrations are applied. Finally, figure 15c shows that the angular frequency drops significantly for low values of Gs (in the range of Gs where Gr_c decreases) and then undergoes a growth phase when the Gershuni number is further increased.

The variations with Gs of the contributions to the fluctuating kinetic energy budget for these thermal instabilities are given in figures 17a and 18a. We first notice the rather strong destabilizing (positive) contribution of the buoyancy term K'_b. For the stationary longitudinal mode (Fig. 17a), dominant at low Gs numbers, the initiation of the instability is jointly due to buoyancy K'_b and, to a lesser extent, to shear K'_s. At low Gershuni numbers ($Gs \lesssim 250$), steep variations are observed, corresponding to an increase of the buoyancy term K'_b and a decrease of the shear term K'_s, while the vibration term related to the horizontal temperature gradient K'_{v2} remains weak and negative, therefore slightly stabilizing. These

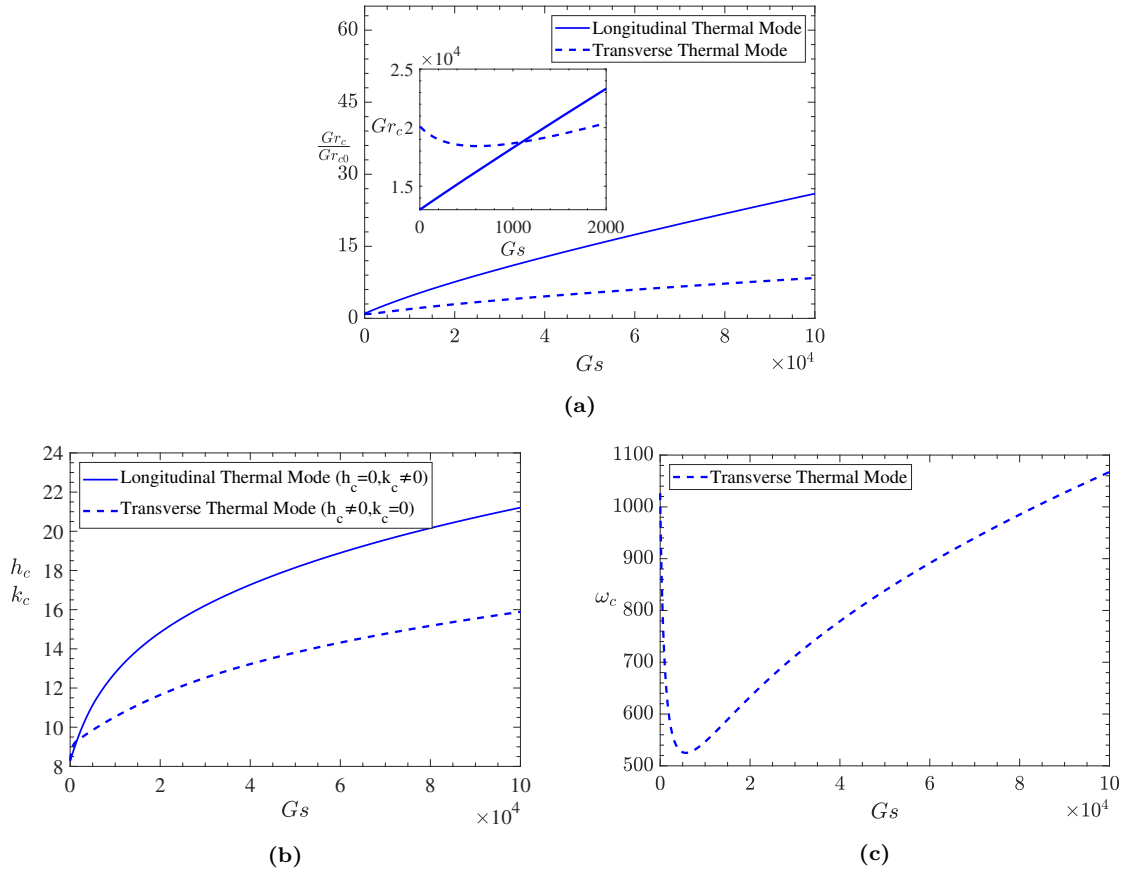

Figure 15: Variation of the critical threshold Gr_c/Gr_{c0} (a), wave numbers h_c and k_c (b), and angular frequency ω_c (c) of the oscillatory transverse mode as a function of the Gershuni number Gs at $Pr = 1$. The inset in (a) gives $Gr_c(Gs)$ at low Gs numbers and highlights the crossing of the critical curves at $Gs \approx 1100$.

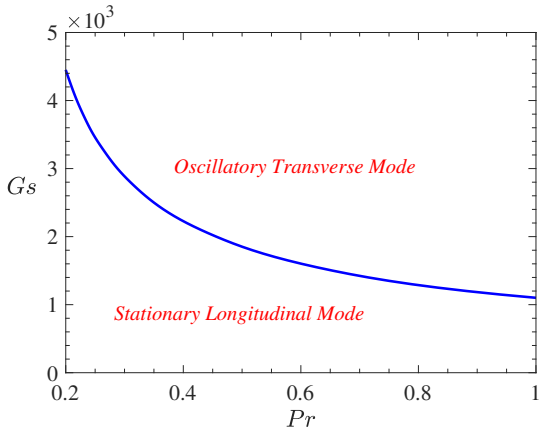

Figure 16: Variation of the transition point between the critical domains of the oscillatory transverse and the stationary longitudinal modes in the (Gs, Pr) space.

variations can be connected with the initial decrease of Gr_c. In contrast, when Gs is further increased, all the terms evolve in the opposite ways, with an increasing destabilizing participation of the term due to vibrations K'_{v2} and a decreasing/increasing contribution of the buoyancy/shear term K'_b/K'_s. All the contributions then participate to the destabilization, and at $Gs = 10^5$, for example, K'_b and K'_s have similar contributions close to 0.4, while $K'_{v2} \approx 0.19$.

For the oscillatory transverse mode (Fig. 18a), we can clearly observe that the contributions of the shear term K'_s and of the vibration term associated with the longitudinal temperature gradient K'_{v2} remain weak and therefore do not participate in the global balance. The dominant contribution without vibration ($Gs = 0$) is due to the buoyancy term K'_b, but this contribution strongly decreases for small Gs numbers, in connection with the steep increase of the vibration term associated with the vertical

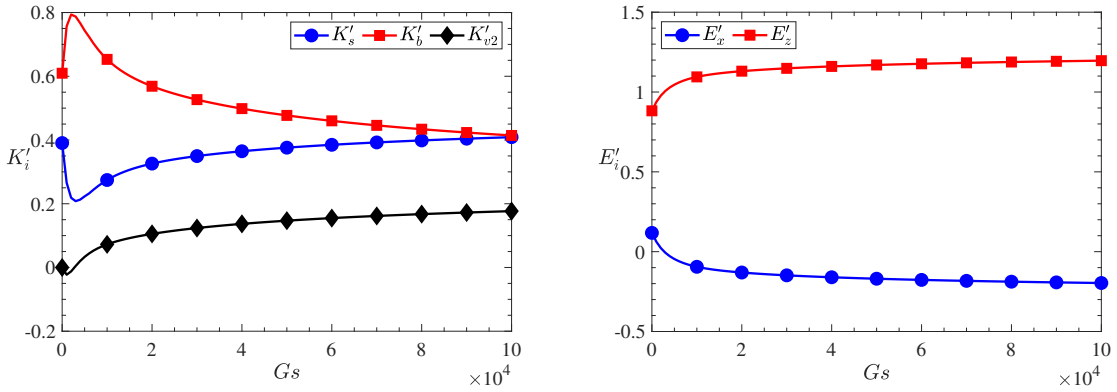

(a) **(b)**

Figure 17: Contributions to the fluctuating kinetic energy (a) and fluctuating thermal energy (b) as a function of the Gershuni number Gs for the stationary longitudinal thermal mode at $Pr = 1$.

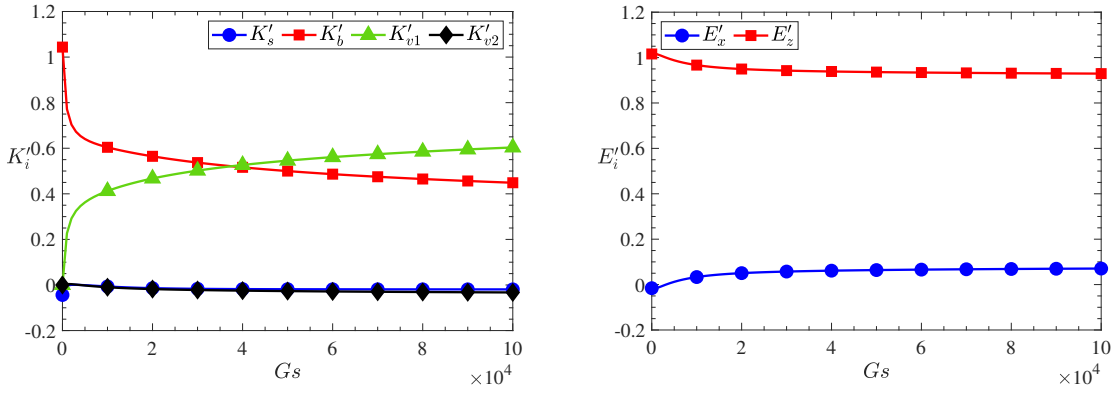

(a) **(b)**

Figure 18: Contributions to the fluctuating kinetic energy (a) and fluctuating thermal energy (b) as a function of the Gershuni number Gs for the oscillatory transverse thermal mode at $Pr = 1$.

temperature gradient K'_{v1}. These variations persist when Gs is further increased, but in a smoother way. Finally, both buoyancy term K'_b and vibration term K'_{v1} contribute to the destabilization, K'_{v1} even becoming dominant for $Gs > 4 \times 10^4$.

The variations with Gs of the contributions to the fluctuating thermal energy budget for the thermal instabilities are given in figures 17b and 18b. We observe that the main contribution is E'_z, linked to the vertical gradient of temperature, indicating that both these instability modes are directly connected with the unstable temperature stratification in the wall regions. The vibrations lead to an increase of E'_z for the stationary longitudinal mode and a decrease for the oscillatory transverse mode. These variations mainly occur below $Gs = 2000$, before a slower asymptotic variation. The term related to the longitudinal gradient of temperature E'_x, which remains weak, evolves conversely with Gs, becoming slightly stabilizing (negative) in the case of the stationary longitudinal mode and slightly destabilizing (positive) in the case of the oscillatory transverse mode.

6 Conclusion

In this study, we investigated the effects of high-frequency vibrations on the linear stability of the natural convection flow driven by a horizontal temperature gradient between two infinite horizontal walls, commonly known as the Hadley circulation.

We first analytically determined the steady-state profiles obtained when horizontal high-frequency vibrations are applied, for two situations corresponding to thermally insulating walls and thermally conducting walls. Regardless of the thermal boundary conditions, the basic steady flow is proportional to the Grashof number Gr and decays when the cavity is subjected to the horizontal vibrations, whose intensity is quantified by the Gershuni number Gs. This decay is more important in the case of insulating walls where the mean kinetic energy of the flow follows a $Gs^{-7/4}$ law compared to the case of conducting

walls where a $Gs^{-5/4}$ law is obtained. The corresponding decay laws for the velocity will be $U_{I-BC} \sim Gs^{-7/8}$ and $U_{C-BC} \sim Gs^{-5/8}$, respectively, and these laws do not depend on the Prandtl number Pr. Analytical expressions are also obtained for the temperature profiles, which are proportional to the product $Gr\,Pr$ and also decrease in intensity with Gs. These temperature profiles differ according to the thermal boundary conditions, in particular with an unstable temperature stratification near the horizontal walls in the case of thermally conducting boundary conditions.

Our linear stability analysis has shown that high-frequency horizontal vibrations have a stabilizing effect on all instabilities that may develop in the cavity for small and moderate Prandtl numbers. At very low Prandtl numbers where the temperature is difficultly perturbed, a two-dimensional stationary shear instability related to the inflectional character of the velocity profile is generally obtained. This instability is strongly stabilized when the vibrations are applied, so that the domain of Pr where it appears shrinks with the increase of Gs. This effect is also more pronounced in the case of thermally insulating walls (for which the basic flow decreases more rapidly) than in the case of thermally conducting walls. At low Prandtl numbers, a three-dimensional oscillatory instability linked to the competition between the buoyancy and the inertia of the fluid particles is favored. With the vibrations, the region of Pr where this instability is dominant becomes larger and is rather shifted towards smaller Prandtl numbers. Finally, for larger Prandtl numbers, the nature of the dominant instability depends on the thermal boundary conditions, but, in any case, the perturbations are localized in the same region, near the horizontal walls. Indeed, a three-dimensional shear instability appearing as longitudinal rolls is obtained for insulating walls while a thermal instability sets in for conducting walls in connection with the unstable temperature stratification near the walls. However, this thermal instability corresponds to three-dimensional longitudinal rolls for small Gershuni numbers and to two-dimensional oscillatory transverse rolls when the Gershuni number is sufficiently increased. For these instabilities obtained for moderate Prandtl numbers, the domains where they are dominant also increase by extending towards smaller Prandtl numbers.

An energy analysis of the disturbances at the instability thresholds was also conducted. This analysis showed that the contributions of the high-frequency vibrations to the fluctuating kinetic energy through the perturbed vibration force depend on the instability under consideration: the horizontal vibrations contribute as a stabilizing effect for the oscillatory instability, a destabilizing effect for the two-dimensional stationary shear instability developing at very low Prandtl numbers as well as for the thermal instabilities developing for conducting walls, and a neutral effect in the case of the three-dimensional stationary shear instability developing for insulating walls. The stabilizing effect observed for all these instabilities when Gs is increased, is then not due to the only influence of the perturbed vibration force, but is also strongly connected with the decay of the basic flow (velocity and temperature) when the cavity is submitted to the horizontal high-frequency vibrations. The fact that such decay of the base flow is stronger in the case of thermally insulating walls generally induces a better stabilization of the instabilities in this case.

Acknowledgement

This collaborative work was supported by the PHC Maghreb Partnership Program No. 36951NG.

Declaration of Interests. The authors report no conflict of interest.

Data availability

The data that support the findings of this study are available from the corresponding author upon reasonable request.

References

Bardan, G. and Mojtabi, A. (2000). On the Horton–Rogers–Lapwood convective instability with vertical vibration: Onset of convection. *Phys. Fluids*, 12(11):2723–2731.

Benzid, C., Kaddeche, S., Abdennadher, A., Henry, D., and Ben Hadid, H. (2009). Rayleigh-Bénard instabilities under high-frequency vibration and magnetic field. *C. R. Mecanique*, 337:291–296.

Birikh, R. V. and Katanova, T. N. (1998). Effect of high-frequency vibrations on the stability of advective flow. *Fluid Dyn.*, 33(1):12 – 17.

Bouarab, S., Mokhtari, F., Kaddeche, S., Henry, D., Botton, V., and Medelfef, A. (2019). Theoretical and numerical study on high frequency vibrational convection: Influence of the vibration direction on the flow structure. *Phys. Fluids*, 31:043605.

Bouarab, S., Mokhtari, F., Kaddeche, S., Henry, D., Botton, V., and Medelfef, A. (2020). Effect of high frequency vibrations on PV silicon purification. *J. Cryst. Growth*, 529:125298.

Capper, P. and Zharikov, E. (2015). Handbook of crystal growth. Handbook of Crystal Growth, pages 951–993. Elsevier, Boston, second edition edition.

Chikulaev, D. G. and Shvarts, K. G. (2015). Effect of rotation on the stability of advective flow in a horizontal liquid layer with solid boundaries at small Prandtl numbers. *Fluid Dyn.*, 50:215–222.

Cisse, I., Bardan, G., and Mojtabi, A. (2004). Rayleigh-Bénard convective instability of a fluid under high-frequency vibration. *International Journal of Heat and Mass Transfer*, 47(19):4101–4112.

Crewdson, G. and Lappa, M. (2022). Spatial and temporal evolution of three-dimensional thermovibrational convection in a cubic cavity with various thermal boundary conditions. *Phys. Fluids*, 34(1):014108.

Delgado-Buscalioni, R. and Crespo del Arco, E. (1999). Stability of thermally driven shear flows in long inclined cavities with end-to-end temperature difference. *Int. J. Heat Mass Transf.*, 42(15):2811 – 2822.

Demin, V., Gershuni, G., and Verkholantsev, I. (1996). Mechanical quasi-equilibrium and thermovibrational convective instability in an inclined fluid layer. *Int. J. Heat Mass Transfer*, 39(9):1979–1991.

Dhanaraj, G., Byrappa, K., Prasad, V., and Dudley, M. (2010). *Springer handbook of crystal growth.* Springer, Berlin, Heidelberg.

Dridi, W., Henry, D., and Ben Hadid, H. (2008). Influence of acoustic streaming on the stability of melt flows in horizontal Bridgman configurations. *J. Cryst. Growth*, 310:1546–1551.

Dridi, W., Henry, D., and Ben Hadid, H. (2010). Stability of buoyant convection in a layer submitted to acoustic streaming. *Phys. Rev. E*, 81:056309.

Farooq, A. and Homsy, G. M. (1994). Streaming flows due to g-jitter-induced natural convection. *J. Fluid Mech.*, 271:351–378.

Farooq, A. and Homsy, G. M. (1996). Linear and nonlinear dynamics of a differentially heated slot under gravity modulation. *J. Fluid Mech.*, 313:1–38.

Fu, W. S. (1993). Transient thermal convection in an enclosure induced simultaneously by gravity and vibration. *Int. J. Heat Mass Transfer*, 36(2):437–452.

Gershuni, G. and Zhukhovitskii, E. (1963). On parametric excitation of convective instability. *J. Appl. Math. Mech.*, 27(5):1197–1204.

Gershuni, G. Z., Laure, P., Myznikov, V., Roux, B., and Zhukhovitsky, E. M. (1992). On the stability of plane-parallel advective flows in long horizontal layers. *Microgravity Q.*, 2:141–151.

Gershuni, G. Z. and Lyubimov, A. V. (1998). *Thermal Vibrational Convection.* John Wiley & Sons.

Gershuni, G. Z. and Zhukhovitskii, E. M. (1981). Convective instability of a fluid in a vibration field under conditions of weightlessness. *Fluid Dyn.*, 16(4):498–504.

Gershuni, G. Z., Zhukhovitskii, E. M., and Yurkov, I. S. (1970). On convective stability in the presence of periodically varying parameter. *J. Appl. Math. Mech.*, 34(3):442–452.

Gershuni, G. Z., Zhukhovitsky, E. M., and Yurkov, I. S. (1982). Vibrational thermal convection in a rectangular cavity. *Fluid Dyn.*, 17:565–569.

Gresho, P. M. and Sani, R. L. (1970). The effects of gravity modulation on the stability of a heated fluid layer. *J. Fluid Mech.*, 40(4):783–806.

Hadley, G. S. (1735). Concerning the cause of the general trade winds. *Phil. Trans.*, 29:58–62.

Hart, J. E. (1972). Stability of thin non-rotating Hadley circulations. *J. Atmos. Sci.*, 29:687–696.

Henry, D., Kaddeche, S., and Ben Hadid, H. (2005). Stabilization of thermogravitational flows by magnetic field and surface tension. *Phys. Fluids*, 17:054106.

Hudoba, A. and Molokov, S. (2018). The effect of the Prandtl number on magnetoconvection in a horizontal fluid layer. *Int. J. Heat Mass Transf.*, 116:1292–1303.

Hudoba, A., Molokov, S., Aleksandrova, S., and Pedcenko, A. (2016). Linear stability of buoyant convection in a horizontal layer of an electrically conducting fluid in moderate and high vertical magnetic field. *Phys. Fluids*, 28:094104.

Kaddeche, S., Garandet, J., Henry, D., Hadid, H. B., and Mojtabi, A. (2015). On the effect of natural convection on solute segregation in the horizontal bridgman configuration: Convergence of a theoretical model with numerical and experimental data. *J. Cryst. Growth*, 409:89–94.

Kaddeche, S., Henry, D., and Ben Hadid, H. (2003). Magnetic stabilization of the buoyant convection between infinite horizontal walls with a horizontal temperature gradient. *J. Fluid Mech.*, 480:185–216.

Kuo, H. P. and Korpela, S. A. (1988). Stability and finite amplitude natural convection in a shallow cavity with insulated top and bottom and heated from a side. *Phys. Fluids*, 31(1):33–42.

Lagarias, J. C., Reeds, J. A., Wright, M. H., and Wright, P. E. (1998). Convergence properties of the Nelder-Mead simplex method in low dimensions. *SIAM Journal of Optimization*, 9:1.112–1.147.

Lappa, M. (2007). Secondary and oscillatory gravitational instabilities in canonical three-dimensional models of crystal growth from the melt. Part 2: Lateral heating and Hadley circulation. *C. R. Mécanique*, 335:261–268.

Lappa, M. (2012). Exact solutions for thermal problems: Buoyancy, Marangoni, Vibrational and Magnetic-field-controlled flows. *Rev. Applied Phys.*, 1(1):1–14.

Laure, P. (1987). Étude des mouvements de convection dans une cavité rectangulaire soumise à un gradient de température horizontal. *J. Theo. App. Mechanics*, 6:351–382.

Laure, P. and Roux, B. (1989). Linear and non-linear analysis of the Hadley circulation. *J. Cryst. Growth*, 97:226–234.

Lizée, A. and Alexander, J. I. D. (1997). Chaotic thermovibrational flow in a laterally heated cavity. *Phys. Rev. E*, 56:4152–4156.

Lyubimov, D., Lyubimova, T., Meradji, S., and Roux, B. (1997). Vibrational control of crystal growth from liquid phase. *J. Cryst. Growth*, 180(3):648–659.

Lyubimova, T., Lyubimov, D., and Ivantsov, A. (2014). The influence of vibrations on melt flows during detached Bridgman crystal growth. *J. Cryst. Growth*, 385:77–81.

Mathews, J. H. and Fink, K. D. (1999). *Numerical methods using Matlab*. Prentice Hall.

Medelfef, A., Henry, D., Bouabdallah, A., Kaddeche, S., and Boussaa, R. (2017). Effect of rotation on the stability of side-heated buoyant convection between infinite horizontal walls. *Phys. Rev. Fluids*, 2:093902.

Mialdun, A., Ryzhkov, I. I., Melnikov, D. E., and Shevtsova, V. (2008). Experimental evidence of thermal vibrational convection in a nonuniformly heated fluid in a reduced gravity environment. *Phys. Rev. Letters*, 101:084501.

Mokhtari, F., Kaddeche, S., Henry, D., Bouarab, S., Medelfef, A., and Botton, V. (2020). Three-dimensional effect of high frequency vibration on convection in silicon melt. *Phys. Rev. Fluids*, 5:123501.

Naumann, R., Haulenbeek, G., Kawamura, H., and Matsunaga, K. (2002). The JUSTSAP experiment on STS-95. *Microgravity sci. Technol.*, 13(22):22 – 32.

Nelder, J. A. and Mead, R. (1965). A simplex method for function minimization. *Comput. J.*, 7:308–313.

Perez-Espejel, D. and Avila, R. (2019). Linear stability analysis of the natural convection in inclined rotating parallel plates. *Phys. Lett. A*, 383(9):859–866.

Perminov, A. V., Nikulina, S. A., and Lyubimova, T. P. (2022). Analysis of thermovibrational convection modes in square cavity under microgravity conditions. *Microgravity Sci. Technol.*, 34:34.

Pimputkar, S. M. and Ostrach, S. (1981). Convective effects in crystals grown from melts. *J. Cryst. Growth*, 55:614–646.

Rogers, J. L., Schatz, M. F., Bougie, J. L., and Swift, J. B. (2000). Rayleigh-Bénard convection in a vertically oscillated fluid layer. *Phys. Rev. Lett.*, 84:87–90.

Shevtsova, V., Gaponenko, Y. A., Melnikov, D. E., Ryzhkov, I. I., and Mialdun, A. (2010). Study of thermoconvective flows induced by vibrations in reduced gravity. *Acta Astronaut.*, 66:166 – 173.

Shvarts, K. and Boudlal, A. (2010). Effect of rotation on stability of advective flow in horizontal liquid layer with a free upper boundary. *Journal of Physics: Conference Series*, 216:012005.

Shvarts, K. G. (2005). Effect of rotation on the stability of advective flow in a horizontal fluid layer at a small Prandtl number. *Fluid Dyn.*, 40:193–201.

Swaminathan, A., Garrett, S. L., Poese, M. E., and Smith, R. W. M. (2018). Dynamic stabilization of the Rayleigh-Bénard instability by acceleration modulation. *J. Acoust. Soc. Am*, 144(4):2334–2343.

Zyuzgin, A. V., Putin, G. F., and Kharisov, A. F. (2007). Ground modeling of thermovibrational convection in real weightlessness. *Fluid Dyn.*, 42:354–361.